Vol. 62, pp. 821-846 (2024) DOI: 10.3749/2400008

MAGNETIC FABRICS IN LAMINATED ROCKS OF THE ILÍMAUSSAQ IGNEOUS COMPLEX, SOUTHERN GREENLAND

BRIAN O'DRISCOLL§

Department of Earth and Environmental Sciences, University of Ottawa, 150 Louis Pasteur Pr., Ottawa, Ontario K1N 6N5, Canada

MICHAEL S. PETRONIS

Environmental Geology, Natural Resources Management Department, New Mexico Highlands University, P.O. Box 9000, Las Vegas, New Mexico 87701, USA

MICHAEL A.W. MARKS

FB Geowissenschaften, Mathematisch-Naturwissenschaftliche Fakultät, Universität Tübingen, 72074 Tübingen, Germany

WILLIAM J. McCARTHY

School of Earth & Environmental Sciences, University of Saint Andrews, Fife, Queen's Terrace, St Andrews, KY16 9TS, UK

Elisabetta MARIANI

Department of Earth, Ocean and Ecological Sciences, University of Liverpool, Liverpool L69 3GP, UK

CARL T.E. STEVENSON

School of Geography, Earth, and Environmental Sciences, University of Birmingham, Birmingham B15 2TT, UK

PATRICIA L. CLAY

Department of Earth and Environmental Sciences, University of Ottawa, 150 Louis Pasteur Pr., Ottawa, Ontario K1N 6N5, Canada

JOHN W. GEISSMAN

Department of Geosciences, ROC 21, University of Texas at Dallas, Richardson, Texas 75080, USA
Department of Earth and Planetary Sciences, 1 University of New Mexico, Albuquerque, New Mexico 87131, USA

Abstract

Nepheline syenites from the \sim 1.2 Ga Ilímaussaq Complex of southern Greenland are examined to assess the utility of anisotropy of magnetic susceptibility (AMS) fabrics as proxies for silicate petrofabrics. Mineral lamination is a relatively common structural feature in cumulate rocks, including in the Ilímaussaq intrusion, but there is little consensus on the process (or processes) responsible for its formation. The Ilímaussaq AMS data are combined with rock magnetic experiments and electron backscatter diffraction (EBSD) measurements to characterize the magnetic mineralogy and compare the magnetic fabrics obtained to the silicate petrofabric. The data show that Na-amphibole (arfvedsonite) is most likely the dominant control on the AMS fabrics in the coarse-grained nepheline syenites (referred to as kakortokites), and that the AMS fabric is inverse relative to the observed silicate fabric. The EBSD data for a kakortokite sample suggests that the petrofabric is defined by arfvedsonite and is wholly planar, with evidence of only weak cross-lineation of $\bf c$ axes. The fine-grained nepheline syenites (lujavrites), two of which have a well-developed lamination carried by Na-pyroxene (aegirine), appear to have composite AMS fabrics that are considered to be a consequence of a mixed

[§] Corresponding author e-mail address: brian.odriscoll@uottawa.ca

aegirine (normal) and arfvedsonite (inverse) response. The combined datasets shed light on the mechanisms of fabric acquisition in both lithologies. In the kakortokites, the AMS fabrics and silicate crystallographic preferred orientations, as well as the lack of observed microstructural evidence for subsolidus intra-crystal deformation, support models invoking gravitationally controlled crystal mats in the development of the macro-rhythmic layering of these rocks. In the lujavrites, the strong planar fabrics revealed by both the AMS and EBSD datasets, with some evidence of subsolidus deformation, point to fabric formation and perhaps even aegirine crystallization at the postcumulus stage. The combination of EBSD and AMS fabric datasets is a powerful means of deciphering the processes responsible for mineral alignment in igneous cumulates.

Keywords: mineral lamination, lujavrite, kakortokite, anisotropy of magnetic susceptibility, arfvedsonite, Ilímaussaq Complex.

Introduction

Mineral-preferred orientation is a common textural feature of cumulate rocks in layered mafic-ultramafic and nepheline-syenite intrusions. In particular, foliation defined by the arrangement of tabular or platy cumulus minerals oriented parallel or subparallel to layering, i.e., the 'igneous lamination' of Wager & Brown (1968), is observed in numerous layered intrusions. The origin of these fabrics, henceforth referred to here as 'mineral lamination', is not always straightforward to discern but may play an important part in elucidating processes operating in the magmatic systems that solidify to produce layered intrusions. Flow and/or syn-magmatic shearing of the crystal mush might be expected to result in the formation of a lineation in addition to foliation, but mineral lamination commonly occurs without an associated visible lineation or asymmetry. In the absence of a lineation, mineral lamination in layered intrusion cumulates has been attributed to a wide range of primary and secondary magma chamber processes, including in situ crystallization, crystal settling, and compaction (e.g., Wager & Brown 1968, McBirney & Noyes 1979, Larsen & Sørensen 1987, McBirney & Nicolas 1997, Irvine et al. 1998, Meurer & Boudreau 1998a, b, O'Driscoll et al. 2008, Bons et al. 2015, Lindhuber et al. 2015).

Magmatic sedimentation processes capable of producing a mineral lamination include crystal settling and deposition of cumulate from crystal laden density currents. Distinguishing between these two scenarios should not be complicated. Fabrics formed via crystal settling should not be associated with a mineral lineation, whereas those associated with high-energy density currents might produce a preferred orientation of crystal long axes on lamination planes (e.g., lineation of plagioclase in the Upper Zone Skaergaard trough bands; Wager & Deer 1939, Holness 2017a). Important fabric-forming processes are also envisaged to occur at the postcumulus stage, i.e., operating on the crystal mush, although determining the proportion of interstitial melt present (and hence rheology) in such situations is not straightforward (Petford 2009). For example, compaction, producing dominantly planar fabrics, has been considered an important process in fabric development (Irvine *et al.* 1998, Meurer & Boudreau 1998a, b). However, compaction should also leave evidence of intra-crystal solid-state (viscous) deformation in the cumulate microstructural record (Holness *et al.* 2017b). Deformation of the partly solidified crystal mush as a result of collapse or syn-magmatic faulting might result in a simple shear component, leaving behind asymmetric small-scale structures in the layered rocks, as well as the possibility of mineral lineations (McBirney & Nicolas 1997, O'Driscoll *et al.* 2007, 2008). The possibility that relatively early-stage crystal settling or density current-related mineral alignments might be modified or masked by postcumulus processes is also worth considering (*e.g.*, Koopmans *et al.* 2022).

In this study, we applied the anisotropy of magnetic susceptibility (AMS) technique to a suite of variably welllaminated rocks from the Ilímaussaq Complex, southern Greenland (Fig. 1a). The application of the AMS method has proven potential in elucidating the nature and origin of mineral lamination in layered intrusions (e.g., Cruden & Launeau 1994, Launeau & Cruden 1998, O'Driscoll et al. 2007, 2008, Selkin et al. 2014, O'Driscoll et al. 2015, Cheadle & Gee 2017), as it offers a rapid, repeatable, and precise means of measuring the petrofabric of rock samples. The rocks selected for study include kakortokites and lujavrites, which comprise most of the floor and intermediate series of the Ilímaussaq intrusion. The principal aim of this study is to assess the utility of AMS as a petrofabric tool in these mineralogically unusual layered cumulates by comparing the characteristics of the magnetic fabrics to the silicate petrofabric using electron backscatter diffraction (EBSD). Mineral lamination formation in these rocks, particularly in the kakortokites, has been interpreted in the context of a number of different models and little consensus exists as to the magmatic processes responsible (see reviews by Upton et al. 1996 and Marks & Markl 2015). Our combination of petrographic observations, rock magnetic experiments, and EBSD permit our AMS data to be used to provide new insights into the mechanisms of fabric development in the Ilímaussag cumulates.

There is considerable value in furthering our understanding of mineral lamination development in layered

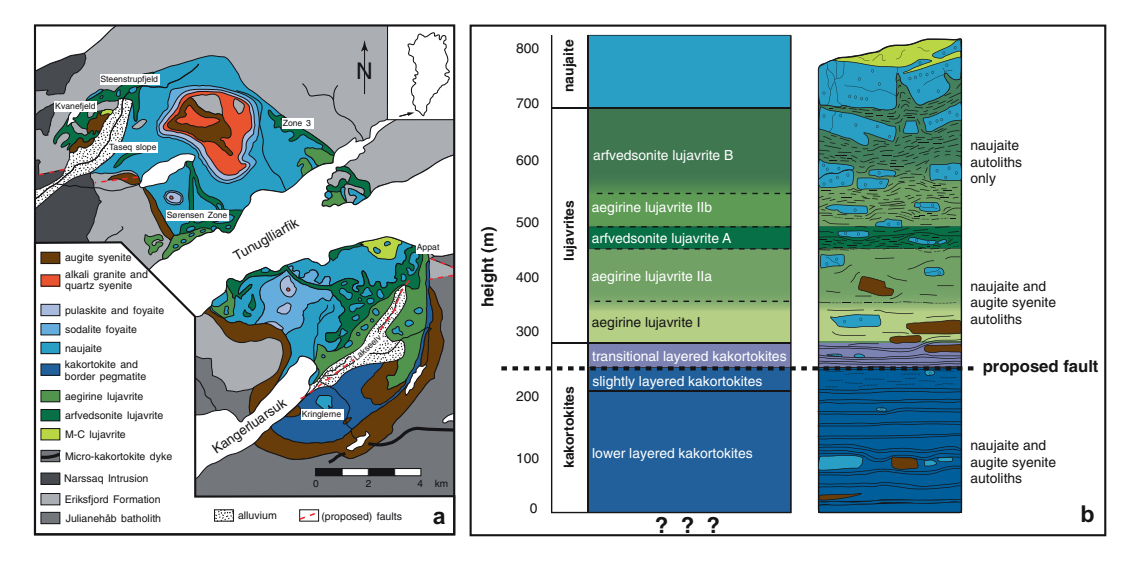


Fig. 1. (a) Simplified geological map of the Ilímaussaq Complex, southeast Greenland (adapted from Marks & Markl 2015, in turn modified from Ferguson 1964, and Sørensen 2001). (b) Generalized stratigraphy of the Ilímaussaq intrusion in its southern part, showing the relationships between the major kakortokite and lujavrite units that are the focus of the present study (modified after Marks & Markl 2015).

intrusions such as the Ilímaussaq intrusion. In addition to shedding light on the rheological behavior of the crystal mush and processes operating in magmatic systems more generally, there are also implications for the compositional evolution of the interstitial melt during mush solidification (cf. Holness et al. 2012, 2017b). Layered intrusions are also associated with some of the most significant magmatic ore (base and precious metal) deposits in the world, and microscale studies on textural and mineral chemical variations in cumulates have revealed useful insights into mineralization processes (e.g., Boudreau 1999, Hanley et al. 2008, Hepworth et al. 2020). The Ilímaussaq layered intrusion hosts some of the largest deposits of REE and U on Earth (Parsons 2012, Marks & Markl 2015), so there may be intrinsic socioeconomic, as well as petrological, insights to be gained in enhancing our understanding of the relative importance of pre-versus postcumulus processes in the microstructural evolution of the Ilímaussag intrusion crystal mush during solidification.

GEOLOGICAL SETTING OF THE ILÍMAUSSAQ COMPLEX

The Ilímaussaq Complex is a 1160 ± 5 Ma (Krumrei et al. 2006) layered intrusion in the Gardar igneous province (southern Greenland; Fig. 1a). It is a composite body, comprising predominantly syenitic-foid rocks, emplaced into the volcano-sedimentary Mesoproterozoic Eriksfjord Formation and the Paleoproterozoic calc-alkaline (granitoid) Julianehåb batholith. Ilímaussaq is the type locality

for agpaitic rocks, which are peralkaline (molar [Na+K]/ Al > 1) rocks that contain Na-Ca-(Ti, Zr)-silicates (e.g., eudialyte; Sørensen 1997, Marks et al. 2011, Marks & Markl 2017) and are highly enriched in alkalis (Li, Na, Rb, Cs), high field strength elements (HFSE; Zr, Hf, Nb, Ta, REE, U, and Th), and halogens (F, Cl, Br, I) (e.g., Bailey et al. 2001). The Ilímaussaq cumulates are believed to be the final products of protracted differentiation of alkali basaltic parental magmas, derived by melt extraction from a lithospheric mantle source (Larsen & Sørensen 1987, Marks et al. 2004, Marks & Markl 2015). Several intrusive phases are recognized: (i) metaluminous augite syenite, (ii) peralkaline granite and quartz syenite, and (iii) volumetrically dominant agnatic nepheline syenites (Larsen & Sørensen 1987). The latter are broadly subdivided into coarse-grained roof series (mostly naujaites) and floor series (kakortokites) cumulates and mostly fine-grained melanocratic rocks (lujavrites) with strong mineral alignments. The kakortokites and lujavrites are the focus of this study. The roof series is envisaged as having been constructed by downward crystallization from the top of the magma chamber and the floor series from the base by accumulation (Marks & Markl 2015). The lujavrites intrude the roof series rocks, but not the floor series cumulates (Fig. 1b).

Medium- to coarse-grained kakortokites comprise the stratigraphically lowest rocks exposed in the floor series (Fig. 1a, b) and are divided into three sub-units (Bohse & Andersen 1981): the lower layered kakortokites (~210 m thick sequence), slightly layered kakortokites $(\sim 35 \text{ m thick})$, and transitional layered kakortokites (~40 m thick). The thick, lower layered kakortokites comprise 29 exposed macro-rhythmic units, with an unknown continuation at depth. The exposed macrorhythmic units are numbered -11 to +17 and are on average \sim 8 m thick, though there is significant variability (Bohse et al. 1971). Overall, these units dip gently toward the center of the intrusion at 10-20°, steepening toward the outer margin to give a bowl-like geometry. Most of the units show modally graded layering at the macroscale as follows: (i) a basal \sim 1 m thick layer dominated by black sodic amphibole [mostly arfvedsonite; NaNa₂(Fe²⁺₄Fe³⁺)Si₈O₂₂(OH)₂], typically characterized by a strong planar mineral lamination, grading upward into (ii) a red eudialyte-rich layer of similar thickness and exhibiting a massive texture, grading in turn into (iii) a topmost weakly laminated alkali feldspar- and nepheline-rich layer \sim 6 m thick. The transition between the three layers within each macro-rhythmic unit are gradational, typically over several tens of centimeters, whereas the contacts between the 29 exposed units are relatively sharp. This sequence is overlain by so-called slightly layered kakortokites. Relatively steeply dipping (45-75° toward NW) transitional layered kakortokites eventually grade upwards into typically fine-grained and melanocratic agpaitic nepheline syenites (lujavrites; Fig. 1b), most of which possess a well-developed mineral lamination (Ferguson 1964, Bohse & Andersen 1981, Andersen et al. 1981, Pfaff et al. 2008, Ratschbacher et al. 2015). The lujavrites are the most evolved rock type in the Ilímaussaq Complex and have been subdivided into aegirine and arfvedsonite lujavrites, depending on the modal abundances of pyroxene (aegirine) and amphibole (arfvedsonite) present (Ferguson 1964, Andersen et al. 1981). In the southern portion of the Ilímaussag intrusion, the lower half of the lujavrite sequence mostly comprises agirine lujavrite, while the upper half is dominated by arfvedsonite lujavrite (Fig. 1a, b).

SAMPLE DESCRIPTIONS AND PETROGRAPHY

Kakortokites

The kakortokite samples analyzed in this study span the upper (white) part of layer +6 to black layer +8 (see Table 1). The kakortokites are mesocumulates to orthocumulates and their mineralogy and texture are described in detail in Lindhuber *et al.* (2015). Information relevant to this study is summarized here, and our sample numbers are the same as in that study. All kakortokites contain the principal cumulus phases arfvedsonite, eudialyte, and alkali feldspar (Fig. 2a, b), as well as a range of other minor and alteration phases (see Figure 3 of Lindhuber *et al.* 2015). Amphibole in the black kakortokites is euhedral, and typically partly (or less commonly fully)

replaced by aegirine (Fig. 2c). It has a bimodal grain size in the black kakortokites, with large (elongate) euhedral prisms (3–5 mm) and relatively small anhedral crystals and a unimodal anhedral nature in the white and red kakortokites. Alkali feldspar has a range of grain sizes, forming large (>5 mm cm long) euhedral plate-like crystals in the white kakortokites. Alkali feldspar in all lithologies exhibits ubiquitous patchy perthitic exsolution and localized alteration to zeolite and analcime (Fig. 2d), though this is less extreme in the white kakortokites.

Mineral lamination is generally well-developed in the black kakortokites and comparatively less well so in the white kakortokites (e.g., Fig. 2a, b). In the former, the lamination is carried by prisms of arfvedsonite and plates of alkali feldspar; both appear to be randomly oriented within the lamination plane. In the white kakortokites, what mineral lamination that is present is carried by alkali feldspar. The alteration of both arfvedsonite and alkali feldspar crystals in the samples studied means that intracrystalline features, including possible twinning, are heavily obscured. Lindhuber et al. (2015) reported that solid-state deformation of arfvedsonite and alkali feldspar crystals is relatively rare. Our observations are in broad agreement with this, though intra-crystal fractures oriented at a high angle to the long axes of arfvedsonite and alkali feldspar are not uncommon (Fig. 2e), as is bending or curvature of relatively elongate crystals of both phases. No visible oxide minerals (e.g., magnetite) occur in any of the kakortokite samples, though trace amounts of sulfides (pyrrhotite, galena, sphalerite) are present in some of the samples.

White layer +6 is ~ 5 m thick, weakly laminated, and consists of ~50 modal percent (mod.%) euhedral alkali feldspar (sample ML-40). Black layer +7 is ~ 1 m thick, contains ~60 mod.% amphibole (ML-35), and exhibits a gradational contact against the underlying white layer. It contains a well-developed mineral lamination, but no evidence of a mineral lineation is visible on lamination planes in this or any other kakortokite sample studied (Fig. 2f, g). Black layer +7 is unusual in that it contains two relatively felsic layers (upper and lower, 3 cm and 15 cm thick, respectively) that have similar mineralogical compositions to the main white layers normally found at the tops of macro-rhythmic units. Samples ML-36 (upper) and ML-37 (lower) are kakortokites collected across the contact zone between white layer +6 and black layer +7, where the two aforementioned thin felsic layers occur and exhibit localized decimeter-scale folding of the layering (Fig. 2h; and see Figure 4 in Lindhuber et al. 2015). Sample ML-36 is a black kakortokite (Fig. 2f), whereas ML-37 samples the contact with black and white kakortokite on either side. White layer +7 (ML-54) comprises \sim 40 mod.% alkali feldspar. The overlying black layer (+8; ML-58) has a sharp basal contact against white layer +7, is relatively eudialyte-rich,

TABLE 1. SAMPLE CHARACTERISTICS AND ANISOTROPY OF MAGNETIC SUSCEPTIBILITY DATA

	Allvedsorme											Ellipsoid
Sample number	(vol.%)	Mineral lamination	×	N* K _{mean} (SI) 1σ**	10**	K_1	K_2	$K_1 \qquad K_2 \qquad K_3$	P_j 1 σ	10	Τ	shape***
Black kakortokites												
ML-35 +7	27	Moderately laminated	12	1.44E-03	7.14E-05	1.009	966.0	0.995	1.016	0.001	-0.725	P (inverse)
ML-36 +7	36	Strongly laminated	9	1.95E-03	4.05E-04	1.014	0.995	0.991	1.025	0.004	-0.667	
ML-58 +8	30	Weakly laminated	2	1.34E-03	8.33E-05	1.011	966.0	0.993	1.019	0.001	-0.687	P (inverse)
Black and white kakortokite												
ML-37 +7	23	Strongly laminated	6	1.05E-03	3.37E-04	1.008	1.000	0.992	1.017	0.003	-0.047	-0.047 P (inverse)
White kakortokites												
ML-40 +6	10	Weakly laminated	9	3.76E-04	3.08E-05	1.004	0.999	0.997	1.007	0.002	-0.351	P (inverse)
ML-54 +7	15	Moderately laminated	7	4.74E-04	4.09E-05	1.005	0.999	0.997	1.011	0.004	-0.014	P (inverse)
Lujavrites												
BR1	15	Strongly laminated	2	7.63E-04	6.02E-05 1.009	1.009	1.001	0.990	1.030	0.012	0.701	O (composite)
BR9	2	Moderately laminated	2	5.38E-04	2.06E-05	1.003	1.000	0.997	1.011	0.012	0.360	O (composite)
BR22	15	Massive	က	7.68E-04	6.39E-05				1.004	0.001	-0.469	P (inverse)

N* Number of sub-specimens per sample.

1σ** Standard error at 1σ level.

Ellipsoid shape*** P, prolate; O, oblate; labeled where suspected inverse or composite fabric.

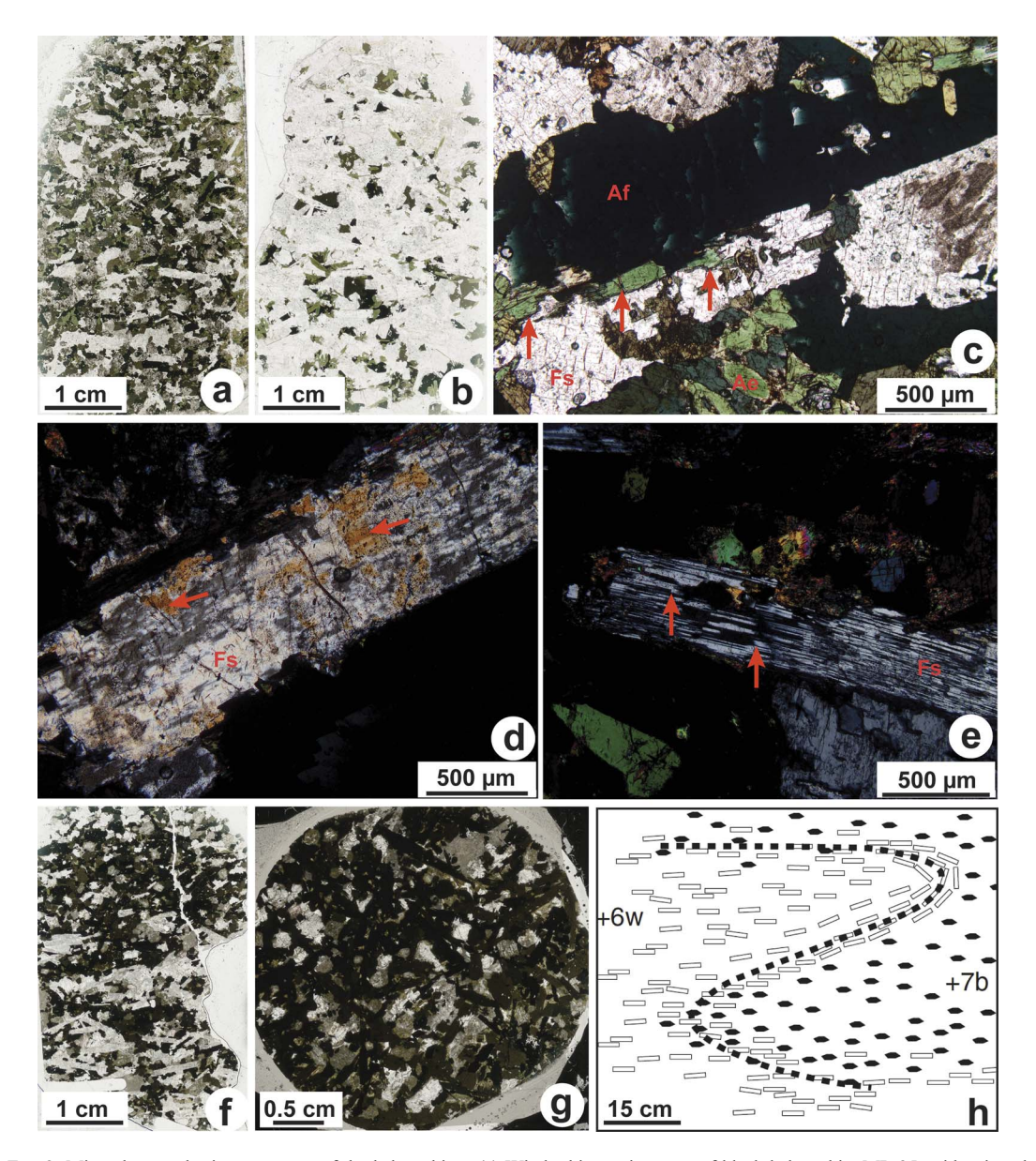


Fig. 2. Mineralogy and microstructures of the kakortokites. (a) Whole thin section scan of black kakortokite ML-35, with mineral lamination (mainly discernible in the alkali feldspar orientation) aligned approximately east—west. (b) Whole thin section scan of white kakortokite ML-54 with weak mineral lamination visible oriented approximately east—west. (c) Plane-polarized light image of arfvedsonite crystal (image center) with smaller aegirine crystals attached to its margins in ML-35 (see red arrows for examples). (d) Cross-polarized light image of patchy perthitic exsolution and alteration in alkali feldspar tablet in sample ML-35. The yellowish colored areas (red arrows) are zeolite (likely natrolite), whereas analcime occurs mainly around the margins of the crystal, which are ragged and irregular. (e) Cross-polarized light image of high angle (to crystal long axis) fractures that appear to offset twin planes in alkali feldspar in sample ML-37 (see red arrows for examples). (f) Thin section scan of sample ML-36, cut perpendicular to mineral lamination plane. The lamination can be observed mainly in the orientation of the euhedral alkali feldspar crystals. (g) Thin section scan of sample (drill core) ML-36, cut parallel to mineral lamination planes. (h) Field sketch, reproduced from Lindhuber et al. (2015), of the fold structure from kakortokite layers +6 and +7, from which samples ML-36 and ML-37 of this study come. See text for further discussion. Abbreviations used in some panels are as follows: Af, arfvedsonite; Ae, aegirine; Fs, alkali feldspar.

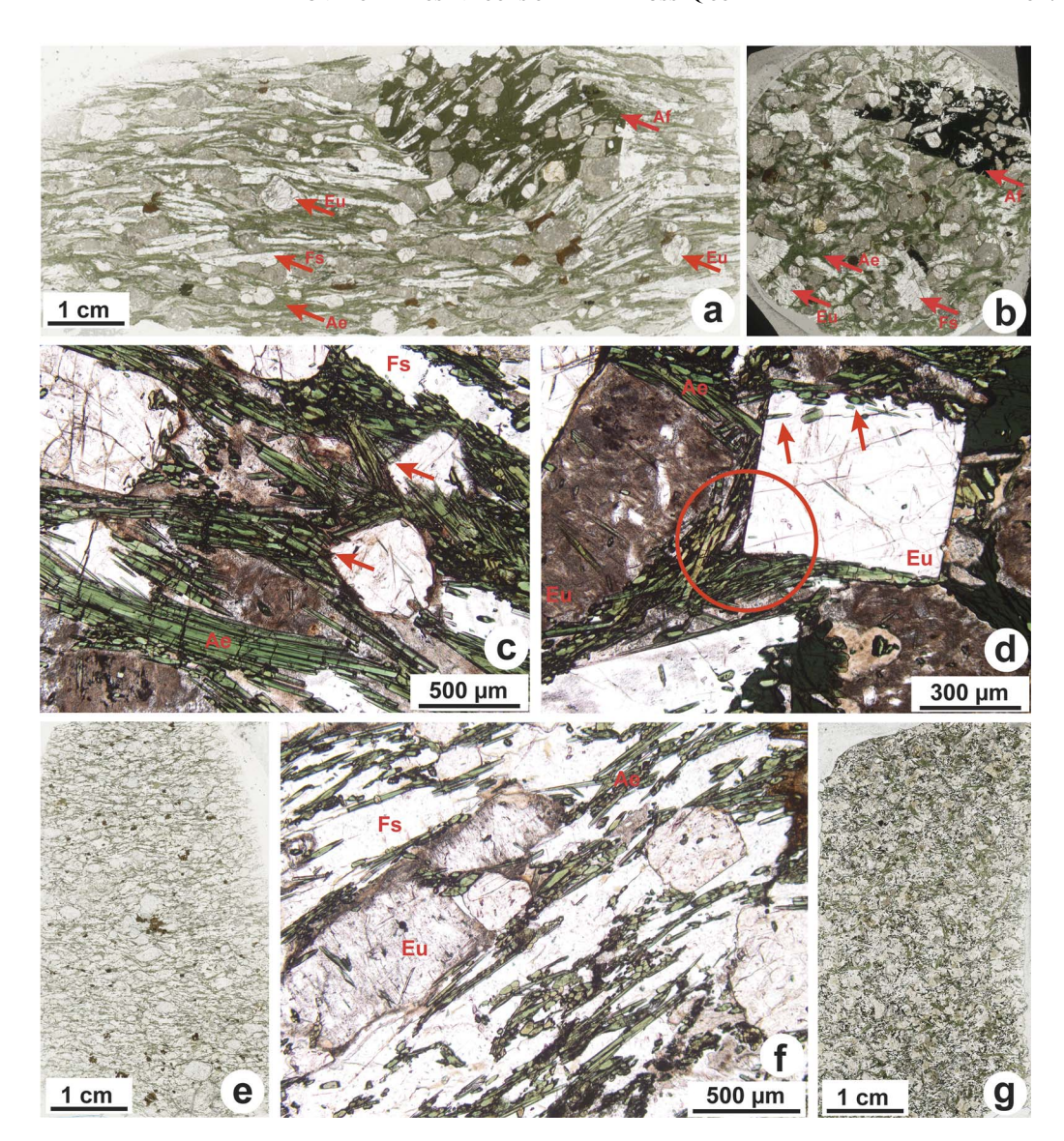


Fig. 3. Mineralogy and microstructures of the lujavrites. (a) Thin section scan, cut perpendicular to mineral lamination planes, of sample BR-1. Mineral lamination is oriented approximately east—west and is carried principally by bunches of aegirine (bottle green color) and alkali feldspar. (b) Thin section scan of sample BR-1, cut parallel to mineral lamination plane. (c) Plane-polarized light image of aegirine-rich laminated zones in sample BR-1, with aegirine wrapping euhedral eudialyte phenocrysts (two examples arrowed). (d) Plane-polarized light photomicrograph of euhedral eudialyte crystal in BR-1, with fine-grained aegirine crystals crosscutting the upper margin of the eudialyte (arrowed). Note also the 'pressure shadow'-like texture (circled) formed by the aegirine lamination adjacent to the eudialyte. (e) Thin section scan, cut perpendicular to mineral lamination planes, of sample BR-9. The mineral lamination, carried principally by aegirine, and which is more weakly developed than that in BR-1, is oriented approximately east—west. Arfvedsonite (anhedral brown-ish-colored crystals) is distributed irregularly throughout the sample. (f) Plane-polarized light photomicrograph of BR-9, showing aegirine mineral lamination in this sample oriented northeast—southwest. One elongate eudialyte crystal is aligned within the lamination, too. (g) Thin section scan of BR-22. Note the lack of an obvious mineral lamination. Abbreviations used in some panels are as follows: Af, arfvedsonite; Ae, aegirine; Eu, eudialyte; Fs, alkali feldspar.

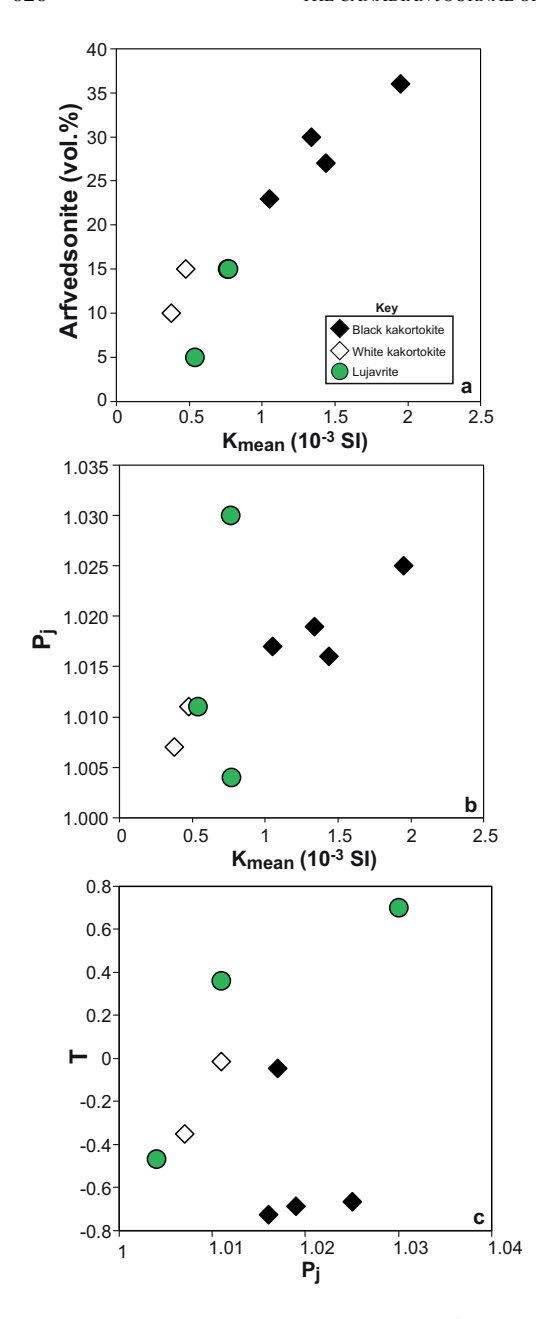


Fig. 4. (a) Plot of arfvedsonite abundance (vol.%) against bulk susceptibility (K_{mean}). Note that lujavrite points for BR-1 and BR-22 overlap each another. (b) Degree of anisotropy (P_j) versus bulk susceptibility (K_{mean}). (c) AMS ellipsoid shape (T) versus degree of anisotropy (P_j). Note that in (a) and (b), K_{mean} values are in 10⁻³ SI. All panels show values for full block sample averages. Color scheme and symbols shown in (a) are the same for all panels. The reader is referred to Table 1 for values plotted.

contains ${\sim}45~\text{mod.}\%$ amphibole, and has a well-developed mineral lamination.

Lujavrites

We studied three samples that exhibit varying strengths of mineral lamination development (Table 1) and are from the lower half of the lujavrite sequence. The character and provenance of these samples are described in more detail in Ratschbacher *et al.* (2015); our sample numbers are the same as used by those authors. No visible oxide phases are present in any of the lujavrites studied here. From well-laminated, to moderately laminated to relatively massive-textured, these samples are BR-1, BR-9, and BR-22, respectively.

Sample BR-1 is a greenish aggirine lujavrite from the aegirine lujavrite I stratigraphic unit (Fig. 1b). It exhibits a strong planar mineral lamination that is unlike the mineral lamination preserved in the kakortokites. The lamination is controlled by the preferred distribution of the c axes of highly prismatic (acicular) aegirine crystals, which are consistently oriented parallel or subparallel to the plane of foliation (Fig. 3a, b, c, d), though appear randomly oriented within that plane (Fig. 3b, d). In planes perpendicular to the lamination, bunches of aggirine crystals anastomose through the sample. Close to eudialyte crystals and arfvedsonite oikocrysts, individual aegirine crystals appear to have shorter and more variable c axis orientations (in the plane of the thin section). Aggirine crystals are commonly observed to wrap around eudialyte crystals and arfvedsonite oikocrysts (Fig. 3c), although aegirine needles do crosscut the outer edges of eudialyte phenocrysts (Fig. 3d). Elongate plates of alkali feldspar also conform to the lamination, but as is also observed for aggirine, show no evidence of lineation within the plane of lamination. The 2-3 cm diameter poikilitic arfvedsonite grains in BR-1 contain alkali feldspar chadacrysts defining their own lamination at a moderateto-high angle to the lamination outside the arfvedsonite oikocrysts (Fig. 3a).

Sample BR-9 is an aegirine lujavrite sampled from the aegirine lujavrite IIA stratigraphic unit. Compared to BR-1, BR-9 has a finer grain size and a smaller proportion of arfvedsonite to aegirine; large oikocrysts like those in BR-1 are not observed. BR-9 exhibits a visible foliation, but this is much weaker than that observed in BR-1 (Fig. 3f, g). No lineation is observed. Sample BR-22 is an arfvedsonite lujavrite from the arfvedsonite lujavrite A unit. This sample has a massive texture, *i.e.*, no mineral alignment is observed in any plane, and a relatively high proportion of fine-grained arfvedsonite is distributed throughout the rock (Fig. 3h; Table 1). No opaque mineral phases were observed during petrographic examination of the lujavrite samples, except for trace ($\ll 1$ vol.%)

amounts of pyrrhotite, pyrite, galena, sphalerite, and löllingite (FeAs₂).

Analytical Techniques

Anisotropy of magnetic susceptibility

Details of the AMS technique as applied to layered intrusion cumulates are described in reviews by O'Driscoll et al. (2008, 2015, and references therein), and the reader is referred to those articles for more details than are provided here. The AMS of a rock is controlled mainly by the preferred orientation of magnetic grains, principally the ferrimagnetic (e.g., magnetite and/or maghemite, if present) and paramagnetic mineral phases (e.g., pyroxene, amphibole). In this study, block samples were drilled in the laboratory and a number of right-cylinder sub-specimens (typically 2–3) of \sim 11 cm³ were extracted from each core; a total of 5-8 sub-specimens were used from each block sample (see Owens 1994). Drilling was carried out perpendicular to the plane of the mineral lamination, as deduced from careful examination of the block samples. The samples were then measured on an AGICO KLY-3S Kappabridge (an induction bridge operating at 300 A/m with a frequency of 875 Hz) at the University of Birmingham (UK). Magnetic susceptibility differences were measured in three orthogonal planes and combined with a measurement of one axial susceptibility to define the second rank AMS tensor.

Assuming that the sub-specimens from each block sample represent a homogeneous multi-normal population, results are reported for block averages of specimen AMS tensors, each normalized by the specimen mean susceptibility. Within-block scatter is characterized through the calculation of 95% confidence limits on directional data and magnitude parameters using a tensor-averaging process (Jelínek 1978, Dunlop & Özdemir 1997, Owens 2000). The magnetic susceptibility tensor, which may be pictured as an ellipsoid, comprises the three principal susceptibility magnitudes ($K_1 \ge K_2 \ge K_3$), and a corresponding set of three orthogonal principal axis directions. The bulk magnetic susceptibility (K_{mean}) is the arithmetic mean of the three principal susceptibility axes intensities. The AMS magnitude parameters adopted in this study are those of Khan (1962) and Jelínek (1981):

$$\label{eq:posterior} {\bm P}_{\bm j} \, = \, \exp\!\sqrt{(2[(\eta 1 - \eta)^2 + (\eta 2 - \eta)^2 + (\eta 3 - \eta)^2])};$$

$$T = (2 \eta 2 - \eta 1 - \eta 3)/(\eta 1 - \eta 3);$$

where $\eta 1 = \ln K_1$, $\eta 2 = \ln K_2$, $\eta 3 = \ln K_3$, and $\eta = \ln(K_1 + K_2 + K_3)^{1/3}$.

The P_j parameter characterizes the strength of the magnetic fabric, such that a value of $P_j=1$ describes

a perfectly isotropic fabric. The shape of the ellipsoid is described by T, which ranges from +1 where purely oblate to -1 where purely prolate and is near zero where triaxial. A plot of T (ellipsoid shape) *versus* P_j (magnetic fabric strength) provides a graphical representation of the shape and strength of the ellipsoid (see Fig. 4c).

Rock magnetic experiments

To characterize the magnetic mineralogy, we conducted a suite of rock magnetic experiments with the principal goal of identifying the mineral(s) that carry the overall remanence, susceptibility, the AMS fabric, and also the quantity, composition, and grain size of the magnetic phase(s) present. Rock magnetic experiments included (1) analysis of low-field susceptibility versus temperature, (2) room temperature susceptibility in variable fields, (3) room temperature hysteresis measurements, (4) magnetic property measurement system (MPMS) analyses, and (5) repeat heating/cooling low-field susceptibility versus temperature experiments. All susceptibility and MPMS experiments were conducted at the New Mexico Highlands University (USA) Paleomagnetic-Rock Magnetic laboratory using an AGICO MFK1-A kappabridge susceptibility meter operating at 200 A/m at 976 Hz and a Quantum Design 7 Tesla MPMS. Hysteresis measurements were conducted with a Princeton Measurements Vibrating Sample Magnetometer (VSM) at the University of Texas at Dallas (USA) paleomagnetism laboratory.

Continuous low-field susceptibility versus temperature measurements were carried out in a stepwise heating/cooling fashion from 25 to 700 to 40 °C in an argon atmosphere using a CS4 furnace attachment for the MFK1-A. These experiments allow for an evaluation of the magnetic mineral composition based on Curie point estimates and assist with revealing mixtures of magnetic phases in a sample (Tauxe 1998). Curie point estimates are typically determined either by the Hopkinson Peak (Hopkinson 1890) or inflection point methods (Tauxe 1998). To investigate potential modification of the magnetic mineral assemblage at high temperature, stepwise reheating lowfield susceptibility versus temperature experiments were carried out on ML-58 (modified after Hrouda 2003, Petronis et al. 2011). In an argon atmosphere, variation of magnetic susceptibility with temperature was first measured from 40 to 540 to 40 °C. The same mass of the powdered sub-specimen was then heated from room temperature to 560 °C and back to 40 °C. Successive runs progressively increased by 20 °C until a maximum of 640 °C was reached, following the same heating and cooling procedure. A final step from 40 to 700 °C was added. Variation in susceptibility with increasing temperature was then evaluated. The room temperature susceptibility experiments in variable fields provide data to evaluate the susceptibility dependence on direct current (DC) applied fields from 2 A/m to 700 A/m using the MFK1-A.

Hysteresis experiments involved vibrating the sample within a 3.0 T applied field at 83 Hz next to a set of pick-up coils. The vibrating sample creates a time varying magnetic flux in the coils, generating a current that is proportional to the sample's magnetization.

The MPMS experiments are used primarily for magnetic mineral identification based on low-temperature crystallographic transitions (e.g., the Verwey transition; Verwey 1939), and for characterizing particle domain size distributions. Two experimental set-ups were used: (1) field cooled (FC) and zero-field cooled (ZFC) and (2) room temperature saturation isothermal remanent magnetization SIRM (RTSIRM) and low-temperature SIRM (LTSIRM). The FC and ZFC measurements were performed by measuring the remanence on warming from 10 K to 300 K. The FC remanence was measured on warming after cooling to 10 K in a 3.0 T field while the ZFC remanence was measured on warming after cooling to 10 K in a zero field. For the RTSIRM, the sample was magnetized at room temperature in a 3.0 T applied field and then the measurement was taken after the field was turned off. The RTSIRM remanence was then measured on cooling from 300 to 10 K. For the LTSIRM, a SIRM was imparted by applying a 3.0 T field at 10 K and then the field was turned off. The LTSIRM remanence was then measured on warming from 10 to 300 K.

Electron backscatter diffraction analysis and mapping

We carried out electron backscatter diffraction (EBSD) analysis in a scanning electron microscope (SEM) on relatively well-laminated samples of both a kakortokite (ML-36) and an aegirine lujavrite (BR-1) in order to quantify any crystallographic preferred orientation (CPO) in the silicate assemblage of these rocks, as well as to aid in the interpretation of the magnetic fabric data. The samples were prepared following the methods of Prior et al. (2009) and Mariani et al. (2009). Chemo-mechanical polishing using colloidal silica was carried out to remove the surface layer damage and to achieve the high-quality surface polishing necessary for EBSD analysis. A thin carbon coat was applied to the samples to avoid any electron charging. All measurements were collected in the Liverpool Earth Science EBSD-SEM laboratory, now part of Liverpool's SEM Shared Research Facility (SRF), using a CamScan X500CrystalProbe field-emission (FE) SEM. Electron backscatter diffraction patterns (EBSP) were obtained using a 20 kV acceleration voltage, 35 nA beam current, and 25 mm working distance. These were automatically indexed using the software package AZtec and then analyzed using AZtec Crystal. Grid spacings between 2 and $25 \, \mu m$ were chosen to map areas between $1500 \times 500 \, \mu m$ (small areas) and $20,000 \times 10,000 \,\mu\text{m}$ (whole thin section), respectively. The microstructure of each of the main phases we studied (aegirine, arfvedsonite, and alkali feldspar) was reconstructed by calculating the orientation difference (disorientation or misorientation) between neighboring data points. The error on orientation measurements is $\pm 0.5^{\circ}$.

Band contrast (BC), all Euler (AE), inverse pole figure (IPF), and phase (Ph) EBSD maps were generated during data analysis to highlight the results obtained. A BC map is a grayscale image of the Kikuchi diffraction pattern (EBSP) quality factor, where dark BC indicates no or poor EBSP quality, whereas bright BC corresponds to good EBSP quality. This map gives a realistic representation of the rock texture analyzed (Prior et al. 2009, Mariani et al. 2009). AE maps visualize crystallographic orientations using a Euler angle-based color scale. Euler angles are determined relative to the SEM reference coordinate system. AE maps display microstructures quantitatively, using color schemes in which similar colors indicate similar crystallographic orientations. IPF orientation maps (X, Y, and Z) use an RGB coloring scheme obtained from inverse pole figure plots and display preferred crystallographic orientations parallel to a selected significant sample direction, such as for example a lineation or stress direction if known. EBSD phase maps show the spatial distribution and relationships of the phases measured.

In this study we used equal area, upper hemisphere stereographic projections (pole figures – PF) to display the CPO of aegirine, arfvedsonite, and feldspar alongside any topotactic relationships between these two minerals. A low multiple of uniform density (MUD) value, illustrated alongside the relevant PF, generally indicates a weak or randomized fabric.

RESULTS

Anisotropy of magnetic susceptibility fabrics

The AMS data for the Ilímaussaq samples are summarized in Figures 4, 5, and 6 and Table 1. The kakortokites have K_{mean} values of 1.05–1.95 \times 10⁻³ SI (black kakortokites) and 0.38–0.47 \times 10⁻³ SI (white kakortokites). A well-developed positive correlation is observed between the bulk magnetic susceptibility and the modal proportion of arfvedsonite across both of these lithologies (Fig. 4a, Table 1). The three lujavrite samples have similar magnetic susceptibilities, with $K_{\text{mean}}\ \text{ranging}$ between 0.54 and 0.77×10^{-3} SI (Fig. 4b). The corrected degree of anisotropy (P_i) ranges between 1.004 (for the massive lujavrite, BR-22) and 1.030 (for the strongly laminated lujavrite, BR-1). The range of P_i for the black and white kakortokites falls between these two extreme values (1.007–1.025). Values of T indicate that the AMS ellipsoids are prolate in all of the kakortokites (-0.014 to -0.725), but the laminated (aegirine-bearing) lujavrites

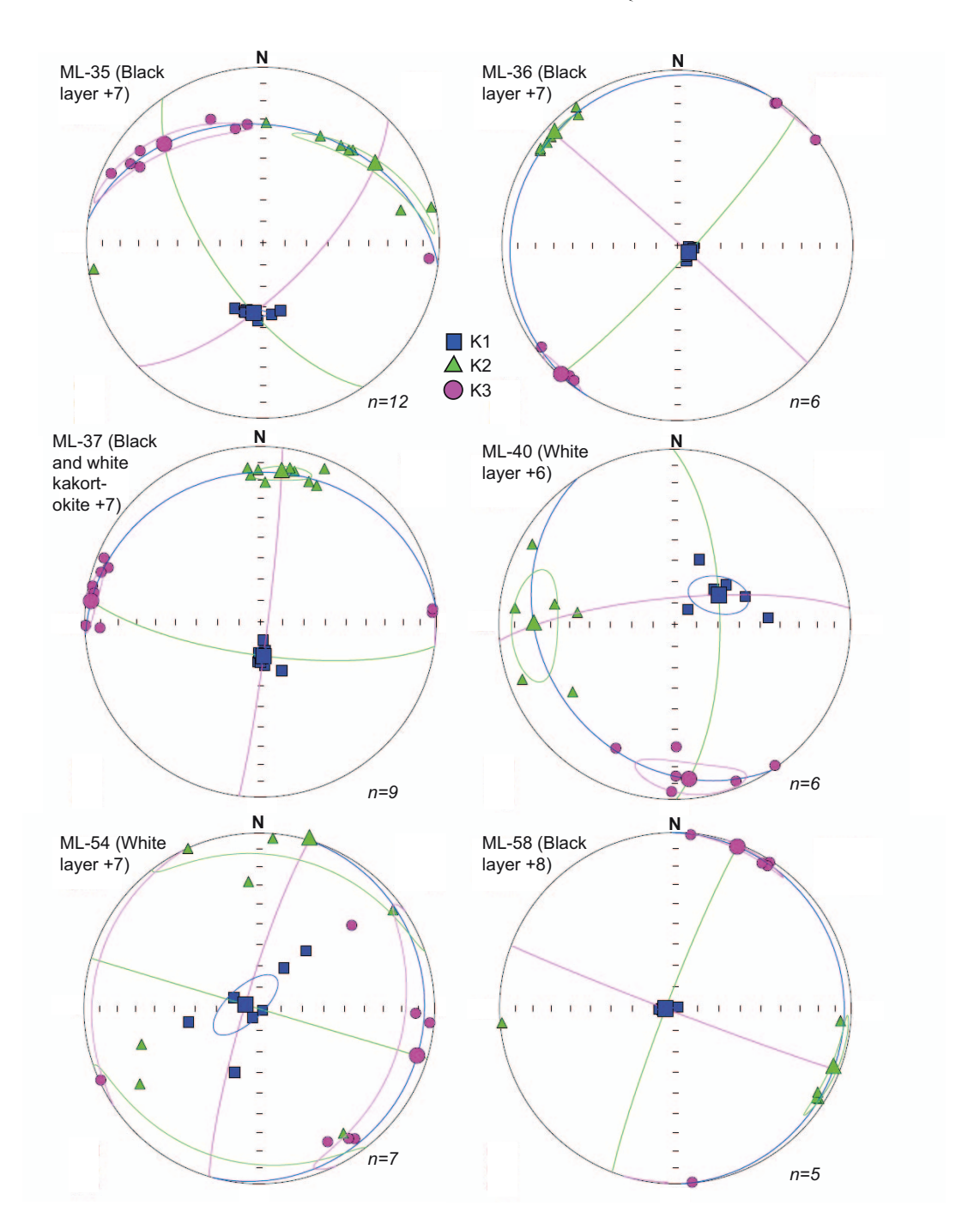


Fig. 5. Lower hemisphere equal area projections of AMS data for the black and white kakortokites. Mean directions of K_1 , K_2 , and K_3 are shown, with associated 95% confidence ellipses. N signifies the top of the projection and has no geographic significance. The numbers of sub-specimens analyzed for each sample are indicated. Each block was drilled perpendicular to the plane of visible mineral lamination, oriented approximately horizontal, and which is thus represented by the outer limit of the projection.

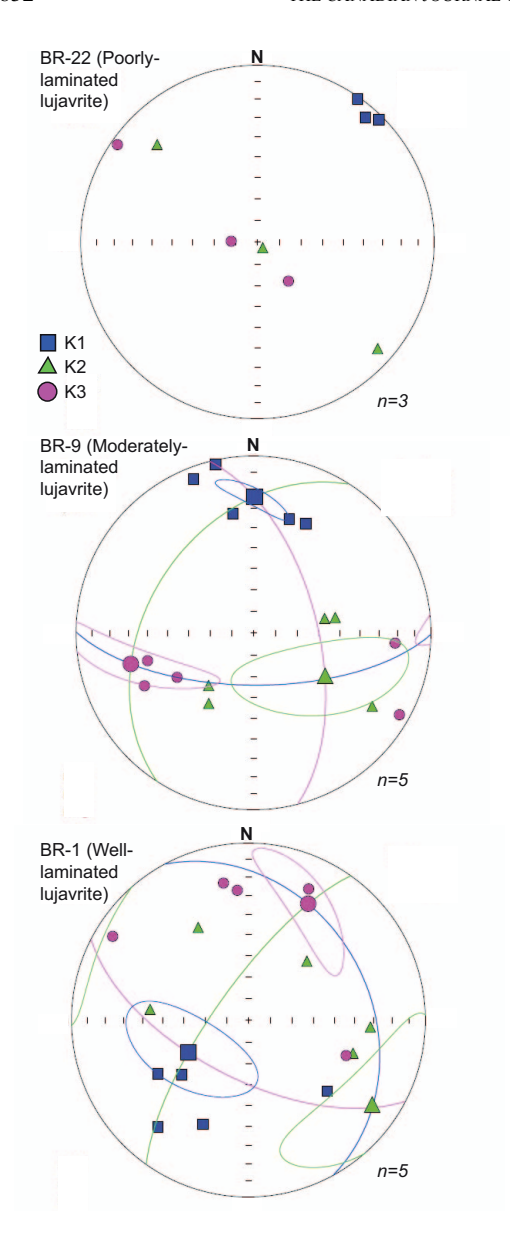


Fig. 6. Lower hemisphere equal area projections of AMS data for the lujavrites. Mean directions of K₁, K₂, and K₃ are shown, with associated 95% confidence ellipses. N signifies the top of the projection and has no geographic significance. The numbers of sub-specimens analyzed for each sample are indicated. Each block was drilled perpendicular to the plane of visible mineral lamination, oriented approximately horizontal, and which is thus represented by the outer limit of the projection. Note that an insufficient number of sub-specimens were obtained from BR-22 to calculate confidence ellipses.

BR-9 and BR-1 have moderately to strongly oblate ellipsoids (T values of 0.360 and 0.701, respectively; Fig. 4c). Sample BR-22 reveals a prolate AMS ellipsoid (T = -0.469).

The AMS data are plotted on lower hemisphere equal area projections in Figures 5 and 6. Because the plane of lamination has been oriented approximately horizontal before drilling, it is delineated by the perimeter (primitive) of these projections. The cumulative uncertainty in lamination orientation resulting from cutting and drilling of the block samples is estimated at $<5^{\circ}$, based on visual inspection of samples during the cutting process and before drilling. The K₁ axis is generally perpendicular to the kakortokite mineral lamination. Samples ML-36, ML-37, ML-54, and ML-58 reveal K₁ that is more or less perpendicular to the silicate foliation, whereas samples ML-35 and ML-40 have K₁ axes that plunge at an angle of up to 30° away from the vertical. Tightly constrained sub-vertical K₁ axes combined with high negative T values show that AMS ellipsoids from the kakortokites are mainly prolate, despite the planar nature of the visible petrofabric (Fig. 5). These observations may be interpreted to reflect inverse magnetic fabrics (Rochette 1988), i.e., where the visible petrofabric elements of the rock, foliation, and lineation (if present) are represented by the K_2 – K_3 plane and K_3 axis, respectively.

In contrast to the kakortokites, the principal susceptibility axes for the lujavrites are less well defined. An insufficient number of sub-specimens (n = 3) were extracted from BR-22 to calculate the 95% confidence ellipses. In both samples BR-1 and BR-9, K_1 is the most well defined susceptibility axis and plunges moderately to shallowly (Fig. 6). The magnetic foliation, defined by the K_1 – K_2 girdle, in both BR-1 and BR-9 appears to be oriented at a moderately high angle to the silicate petrofabric: 30–60° inward from the primitive of the equal area projection.

Rock magnetic characteristics

Continuous low-field susceptibility versus temperature results. The Curie point temperature of stoichiometric magnetite has been shown to decrease with increasing Ti-content (i.e., ulvöspinel) (Readman & O'Reilly 1972, Moskowitz 1981, Nishitani & Kono 1983). Magnetite has a magnetic susceptibility several orders of magnitude greater than paramagnetic mineral phases (Tarling & Hrouda 1993). Low-field susceptibility versus temperature experiments, therefore, provide a quantitative means to estimate mineral composition based on the Curie point estimate(s) for one or more magnetic phases present within the sample. The bulk magnetic susceptibility of all samples is low ($<10^{-3}$ SI volume), which is consistent with a lack of an Fe-Ti oxide phase in these samples and suggests the overall susceptibility is governed by paramagnetic phases (Table 1). All samples yield inferred

Curie point estimates between 561 and 596 °C using either the Hopkinson Peak (Hopkinson 1890) or inflection point methods (Tauxe 1998) (Fig. 7). These temperatures are consistent with the presence of a Fe-Ti oxide phase, although we argue below that this is not a primary magnetic phase that exists in the rocks, but an artifact of the heating experiment, wherein a ferrimagnetic phase grew during heating, even though the tests were conducted in an inert Ar atmosphere. Results of repeat low-field susceptibility versus temperature experiments on sample ML-58 reveal a net \sim 5% increase in magnetic susceptibility following heating to 500 °C (Fig. 8). Subsequent stepwise heating experiments show that the magnetic susceptibility systematically increases in each of the heating experiments, up to the maximum temperature of 700 °C. The data presented in Figure 8 suggest that the Fe-Ti oxide (likely titanian magnetite) grew due to heating and was not present in the natural sample. The conditions of the susceptibility versus temperature experiment may lead to changes in the magnetic phases due to the partially oxidizing environment of the sample holder. Some oxidation occurred due to the presence of O2 on grain surfaces and boundaries within the sample, despite the Ar atmosphere within the sample chamber. Both curves follow similar courses, but the cooling curve is progressively shifted toward higher susceptibility in each step. This often reflects the situation when a new magnetic phase is generated by heating of a less magnetic phase (e.g., Fe-Mg silicate), resulting in a shift in the cooling curve (Irving 1970, Marshall & Cox 1972, Johnson & Atwater 1977, Hrouda 2003). All but one sample (ML-36) exhibit this behavior, i.e., a slight increase in susceptibility on the cooling curve.

Room temperature susceptibility in variable fields. The analysis of the susceptibility in variable fields (2-700 A/m) shows that the samples have no dependence on applied field intensity (Fig. 9). The average bulk susceptibilities in field dependence experiments range between 0.15 and 0.62×10^{-3} SI, in good agreement with the mean susceptibility data collected during AMS analysis and in line with typical values for paramagnetic mineral phases or low concentrations of ferrimagnetic material (e.g., low-Ti titanian magnetite; Tarling & Hrouda 1993). However, even at very low concentrations (<0.01 wt.%), titanian magnetite has a susceptibility that is an order of magnitude greater than the susceptibilities observed in these samples. From the measurement at 30 and 300 A/m, the percentage of field dependence xHd% yields values less than 1% in all cases (average -0.62%). The lack of field dependence is consistent with petrographic observations showing the absence of visible ferrimagnetic (oxide) minerals in these samples (De Wall 2000).

Room temperature hysteresis measurements. Hysteresis experiments were conducted on eight selected samples (Fig. 10). All show a linear increase in magnetization in saturating fields of ± 3.0 Tesla. The width and the degree

of constriction of the hysteresis loops do not vary systematically with increasing applied field. There is no evidence of the presence of a ferrimagnetic phase and these data are interpreted to reflect the dominance of a paramagnetic phase on the magnetic mineralogy of the Ilímaussaq kakortokites and lujavrites.

MPMS results. The MPMS experiments were conducted on representative samples of each lithological type (ML-35, ML-54, ML-58, and BR-22; Fig. 11a, b, c, d). Sample ML-54 shows no decrease or increase in remanence on cooling, indicating that the magnetic moment of the material does not show a dependence on temperature and that the zero field in the chamber is very low (Fig. 11a). The large initial remanence on the warming curve is the LTSIRM and does not reflect a paramagnetic component. The sharp drop between 10 and 50 K may be due to the pyrrhotite transition or to some other unknown phase that disorders or unblocks below 50 K. The (monoclinic) pyrrhotite transition is usually sharp at 35 K (Rochette et al. 1990, 2001), so the former possibility is considered more likely here, given the petrographic observation of accessory pyrrhotite in kakortokites.

Two low-temperature experiments were conducted on sample ML-58: (1) RTSIRM and LTSIRM on a standard sample and (2) a repeat experiment on a concentrate of the magnetic fraction. Both experiments yield nearly identical results (Fig. 11c). On cooling, the remanence remains constant up to ~80 K and falls off rapidly from 80 to 30 K, as observed for ML-54. On warming, similar behavior is also observed to that in sample ML-54. For sample BR-22, we applied a 3.0 T field and cooled (FC) the sample to 10 K and measured the remanence on warming to 300 K (Fig. 11d). We observe a significant loss in remanence from 10 K (1.12 \times 10⁻¹ Am²/kg) to $60 \text{ K} (1.24 \times 10^{-4} \text{ Am}^2/\text{kg})$ followed by an approximately linear decrease in magnetic moment from 70 K (9.86 \times $10^{-5} \text{ Am}^2/\text{kg}$) to 300 K (3.83 × $10^{-5} \text{ Am}^2/\text{kg}$). Similar to ML-54, the sharp drop between 10 and 50 K could be due to the pyrrhotite transition or to an unknown phase that disorders or unblocks below 50 K.

A FC-ZFC experiment was conducted on sample ML-35. Both curves yield identical behavior on warming from 10 to 300 K: a sharp drop between 10 and 60 K and a linear decrease in remanence from 60 to 300 K (Fig. 11b).

In summary, the low-temperature MPMS experiments for the kakortokites show a range of behavior characterized by a loss in remanence over several temperature intervals but little evidence of diagnostic crystallographic phase transitions indicative of the presence of a unique ferrimagnetic or ferromagnetic phase. The lack of low-temperature phase transitions or disordering between 120 and 130 K indicates that these samples do not contain a low Ti-titanian magnetite phase. In addition, there is no evidence of the Morin transition that would reflect the presence of titanian hematite.

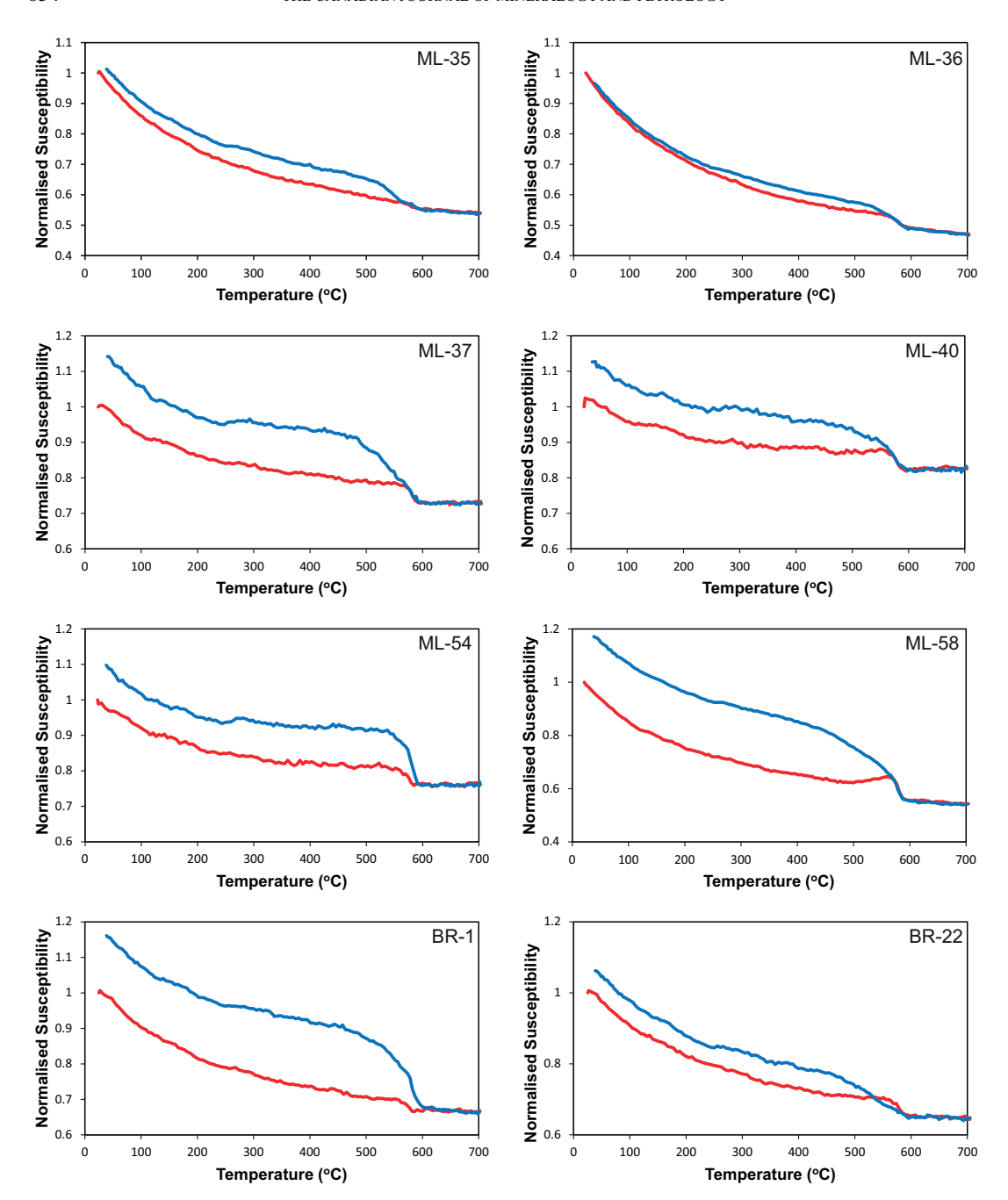


Fig. 7. Continuous (normalized) low-field susceptibility *versus* temperature measurements from room temperature to 700 °C. The red curves are for heating steps and the blue curves are for cooling steps. Curie points of ferromagnetic (*senso lato*) materials are typically estimated using either the inflection point (Tauxe 1998) or Hopkinson Peak methods (Hopkinson 1890). All Ilímaussaq samples yield paramagnetic behavior where the magnetic susceptibility (X) exhibits hyperbolic decay with increasing temperature following the paramagnetic Curie-Weiss law [X = C/(T - T_c)], where C is a material-specific Curie constant, T is absolute temperature, and T_c is the Curie temperature, both in K). No evidence of primary ferromagnetic (s.l.) magnetic phases is observed, although for most samples, a ferromagnetic (s.l.) material did grow from the Fe-Mg silicates in the samples during the heating experiment (see Figure 8 and text for discussion).

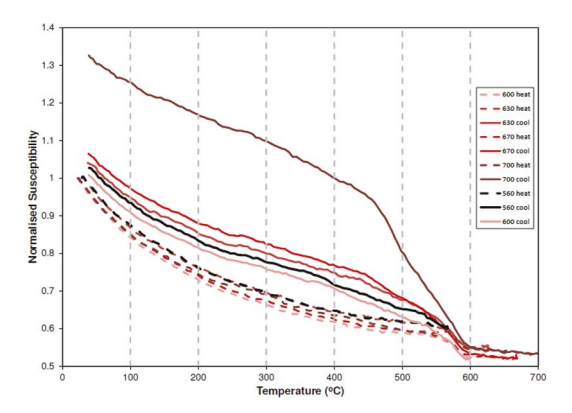


Fig. 8. Stepwise reheating low-field susceptibility *versus* temperature experiments on sample ML-58. The experiments were carried out in an Ar atmosphere, initially from 40 to 540 to 40 °C, and then to progressively higher temperature targets on the same mass of the powdered sub-specimen. A subset (600, 630, 670, and 700 °C) of the sample runs are shown here.

For the RTSIRM and LTSIRM experiments on sample BR-1, the remanence on cooling from 300 to 10 K was measured in a 3.0 T field, and the shape of the curve is close to 1/T, indicative of a paramagnetic phase (Fig. 12a). We model it as a Curie-Weiss paramagnet with M=kH and $k \propto 1/(T-\theta)$, where θ is the 'paramagnetic Curie constant'. For these data, a straight line is fitted on a plot

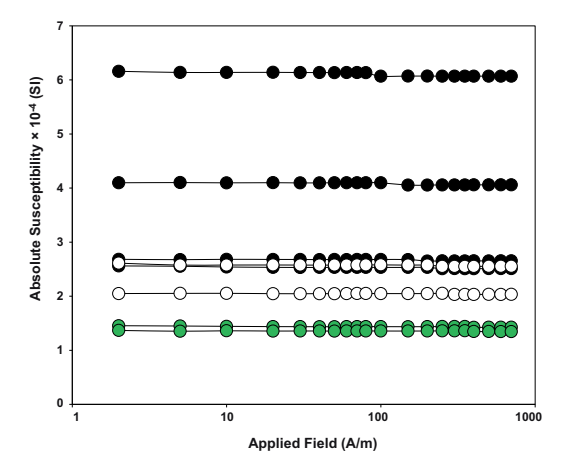


Fig. 9. Room temperature low-field susceptibility experiments in variable fields. These experiments provide data to evaluate the susceptibility dependence on direct current (DC) applied fields from 2 to 700 A/m using the MFK1-A. The analysis indicates that the samples have no dependence on applied field intensity with the average bulk susceptibilities ranging between 0.15 and 0.62 × 10⁻³ SI. The black and white symbols are for black and white kakortokites, respectively, whereas the green symbols represent the lujavrites.

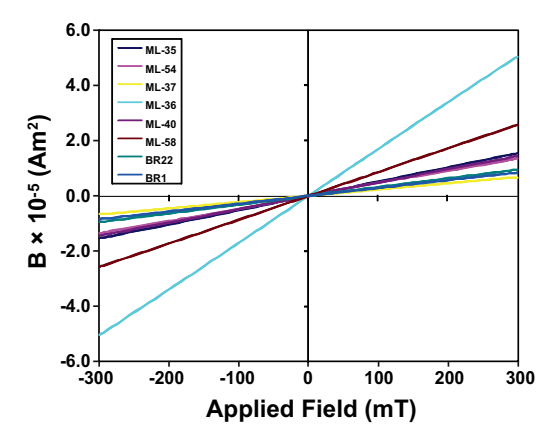


Fig. 10. Hysteresis experiments from eight representative Ilímaussaq samples. The experiment involved vibrating the sample within a 3.0 T peak applied field at 83 Hz. All samples show a linear increase in magnetization to a maximum field of ±3.0 Tesla. The width and the degree of constriction of the hysteresis loops do not vary systematically with increasing applied field. Note that the figure is clipped to 300 mT to clearly show the low-field behavior.

of M versus $1/(T-\theta)$ when θ is ~ -30 K (Fig. 12b). The negative sign of θ indicates that there is a weak antiferromagnetic interaction, possibly reflecting the presence of one of the trace Fe-bearing sulfides (e.g., löllingite) or an unidentified phase.

Electron backscatter diffraction results

The EBSD data for ML-36 and BR-1 are displayed in Figures 13 and 14, respectively. Arfvedsonite is the primary Fe-bearing mineral in ML-36 (Fig. 13c), with subsidiary aegirine, sphalerite, and eudialyte (dark gray areas, not indexed due to poor quality EBSPs). These minerals can be clearly distinguished by differences in microstructure as well as by their crystallographic and diffraction characteristics, such as crystal systems, space groups, and Kikuchi band intensities. The pole figure for ML-36 shows a clear clustering of [010] arfvedsonite axes (MUD = 3.43) perpendicular to the plane of the thin section (Fig. 13b), which is also the lamination plane. Arfvedsonite [001] axes are arranged in a weak cross-lineation pattern in the plane of the sample surface, whereas the [100] axes exhibit a very weak alignment (approximately parallel to the plane of the sample surface). In Figure 13a an IPF map of >1000 arfvedsonite grains highlights that the [100] and [001] axes are contained in the lamination plane and are randomized within it (light green to light blue grains and light blue inset as example orientation). Only a low number of grains display [001] alignment close to the direction of the lamination plane normal (red grains and red inset as example orientation). Aggirine in

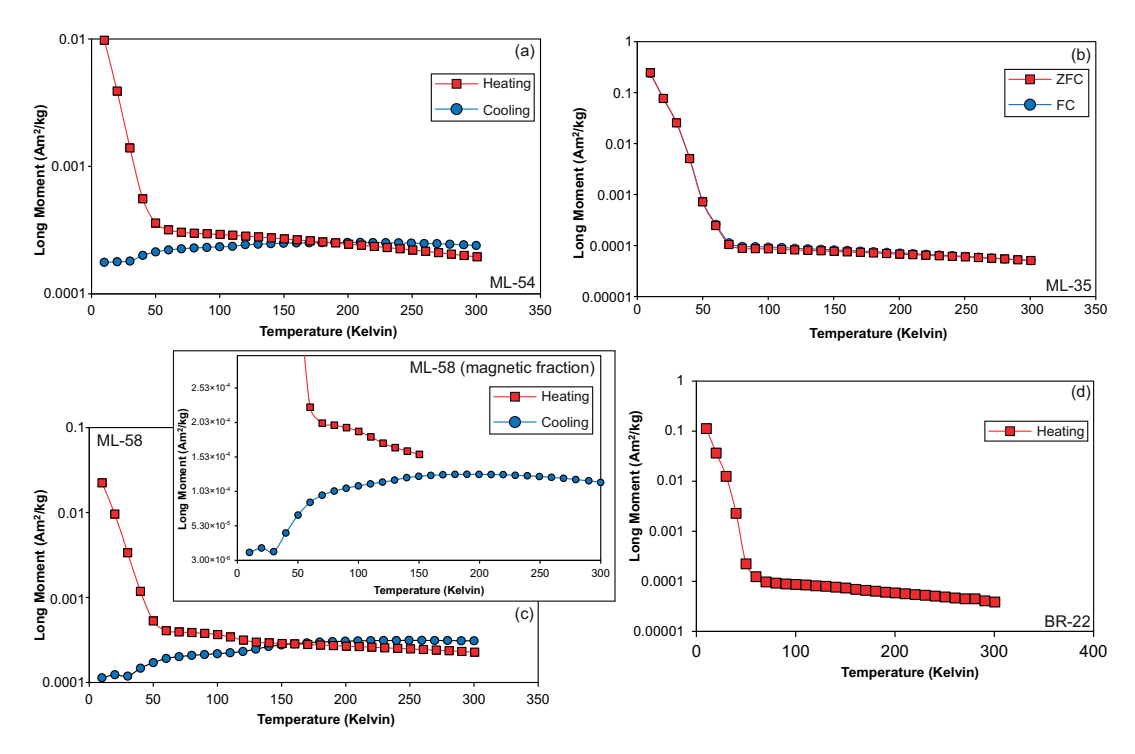


Fig. 11. Results of the Magnetic Properties Measurement System experiments on representative samples from the Ilímaussaq intrusion for samples (a) ML-54, (b) ML-35, (c) ML-58, and (d) BR-22. The two experimental set-ups used were as follows: (1) room temperature saturation isothermal remanent magnetization SIRM (RTSIRM) and low-temperature SIRM (LTSIRM) and (2) field cooled (FC) and zero-field cooled (ZFC). See text for further discussion.

ML-36 is distributed in relatively minor quantities around the edges of arfvedsonite crystals (purple colored phase in Fig. 13c). The pole figure for aegirine indicates the same crystallographic fabric as arfvedsonite, *i.e.*, a strong clustering of [010] axes around the lamination plane normal (Z direction), a relatively weak cross-lineation for [001] in the plane of lamination, suggestive of a decussate texture, and a weak to random orientation distribution of [100] axes (Fig. 13d).

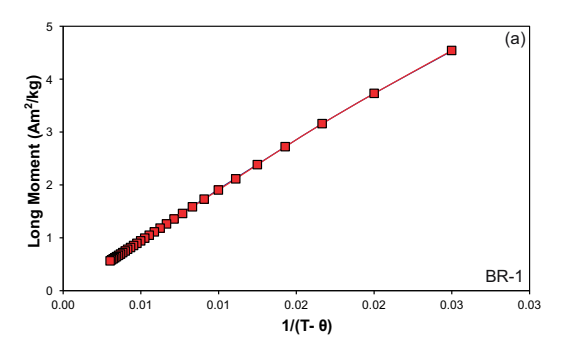
Sample BR-1 contains aegirine, alkali feldspar, and eudialyte as the main rock-forming minerals, with sparse but also coarse-grained patches of arfvedsonite. The phase map of BR-1 (Fig. 14c) suggests that aegirine crosscuts alkali feldspar and also shows the close spatial relationship between these two phases (see also Fig. 14a). Aegirine pole figures reveal strong [100] clustering in the Z direction (MUD = 11), parallel to the lamination plane normal (Fig. 14b). The [010] axes populations form a girdle in the plane of the sample surface (lamination plane) with a very weakly developed clustering observed in the NW–SE direction. Similar to ML-36, the aegirine [001] axes exhibit a weak cross-lineation (NE–SW) suggesting decussate texture. This texture is highlighted in the aegirine IPF Z map, which shows a dominance of red and light

blue orientations (Fig. 14a), and is also represented schematically in the small red and light blue boxes (Fig. 14a). Though constrained by the relatively small number of large grains analyzed within the sample area, the EBSD data show that the alkali feldspars all have [010] parallel to the thin section normal, with [001] and [100] distributed in a girdle within the plane of the lamination (Fig. 14d). The data hint at clustering of the latter two axes, such that alkali feldspar [001] is parallel to the weakly developed maxima observed for [010] in aegirine, and similarly [100] in alkali feldspar is parallel to [001] in aegirine. We also note that pole figures (not shown) for the approximately millimeter sized eudialyte phenocrysts show some clustering of [0001] (c axes) subparallel to the lamination plane normal.

DISCUSSION

Origin of the magnetic fabrics in the kakortokites and lujavrites

The orientation of the AMS susceptibility ellipsoid is controlled by a combination of the shape-preferred orientation and the crystalline and distribution anisotropy



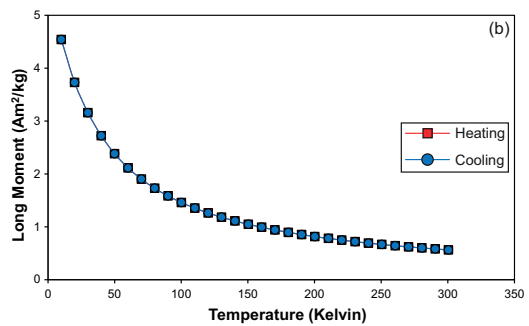


Fig. 12. For sample BR-1, the remanence on cooling and warming from 300 to 10 to 300 K was measured in a 3.0 T field. The shape of the curve is close to 1/T (following the paramagnetic Curie-Weiss Law) and reflects a pure paramagnet (a). This is modeled as a Curie-Weiss paramagnet (b) as described in the text.

of the different ferri/ferromagnetic and paramagnetic mineral phases in a rock (Owens 1974, Rochette et al. 1999). The AMS ellipsoid commonly mimics the petrofabric of the silicate minerals and the fabric is said to be 'normal' (see Borradaile & Jackson 2010, O'Driscoll et al. 2008). Normal magnetic fabric occurs when K₁ is parallel to the structural lineation (e.g., stretching, magma flow, or palaeocurrent lineation) and K₃ is perpendicular to the structural foliation (flattening plane, magmatic foliation, or bedding plane). AMS studies can also reveal 'inverse fabrics' where the K1 and K3 axes are inverted with respect to the silicate petrofabric (Rochette 1988, Ferré 2002) and in other cases, 'intermediate fabrics' are observed where K1 and K2 or K2 and K3 are switched (Ferré 2002). Additional complexity can arise if a composite fabric, comprising 'mixtures' of the above and normal fabrics, is recorded as a single averaged tensor (Parés & van der Pluijm 2002, Parés 2004). To provide context for the Ilímaussag data, the origin and occurrence of inverse and intermediate fabrics is briefly reviewed here.

The term 'inverse magnetic fabric' was originally coined by Rochette (1988), who proposed two possible models: (1) c axis preferred orientation of ferroan carbonate

grains whose maximum susceptibility is parallel to the c axis (see below), and (2) single-domain (SD) elongated ferromagnetic grains. In strongly magnetic minerals (i.e., intrinsic magnetic susceptibility > 1), the easy axis of magnetization parallels the long axis of the grain (i.e., shape anisotropy), and for multidomain (MD) grains a normal magnetic fabric is predicted. In SD grains, the easy axis fixes the direction of the spontaneous magnetization perpendicular to the long axis of the grain, resulting in minimum (near zero) susceptibility along that axis of the grain (Jackson 1991, Rochette et al. 1999). In magnetite- or maghemite-bearing rocks, where SD grains dominate, inverse fabrics are produced (e.g., Potter & Stephenson 1988, Rochette 1988, Borradaile & Puumala 1989, Jackson 1991, Borradaile & Jackson 2004). Borradaile & Jackson (2004) point out that unless SD grains are present in relatively high abundances, mixed or composite fabrics in which the SD 'subfabric' interferes or obscures the MD fabric might be expected. Potter & Stephenson (1988), Rochette (1988), and Borradaile & Puumala (1989) all provide examples of inverse fabrics carried by SD magnetite or maghemite. Superparamagnetic grains may also give rise to inverse magnetic fabrics (Gianalella & Heller 1994). In lower susceptibility, paramagnetic minerals (intrinsic magnetic susceptibility « 1.0 SI) that display crystalline anisotropy, such as phyllosilicate minerals (e.g., biotite), K₃ is parallel to the c axis (i.e., perpendicular to the sheet silicate plane), resulting in a normal magnetic fabric. Normal magnetic fabrics are observed when the dominant magnetic mineral phases are pyrrhotite, hematite, and the phyllosilicates, along with MD magnetite and maghemite.

As summarized by Rochette et al. (1999), some paramagnetic and antiferromagnetic minerals exhibit a minimum susceptibility (K₃) parallel to their long axis that may result in an inverse fabric (e.g., tourmaline, cordierite, and goethite; Rochette et al. 1992). Tourmalinebearing granites consistently exhibit inverse magnetic fabrics (Rochette et al. 1994, Ferré & Améglio 2000). For the Fe-bearing carbonate minerals with maximum susceptibility along their c axis, the origin of the inverse fabric is linked to a preferred orientation of c axes parallel to the shortening direction, resulting from plastic flow of the rhombohedral crystals (see Rochette et al. 1999). Inverse fabrics due to iron-bearing carbonates (e.g., siderite, ankerite, and dolomite and calcite with only 1% substituted Fe₂C) have been described in tectonically deformed limestones by Rochette (1988), Ihmlé et al. (1989), and Ellwood et al. (1986), while Hirt & Gehring (1991) and Winkler et al. (1996) argued for inverse fabrics with a compaction-related origin. Inverse fabrics have not, to our knowledge, been previously reported for arfvedsonite or, indeed, for any igneous rock dominated by amphibole, although Biedermann et al. (2018) noted

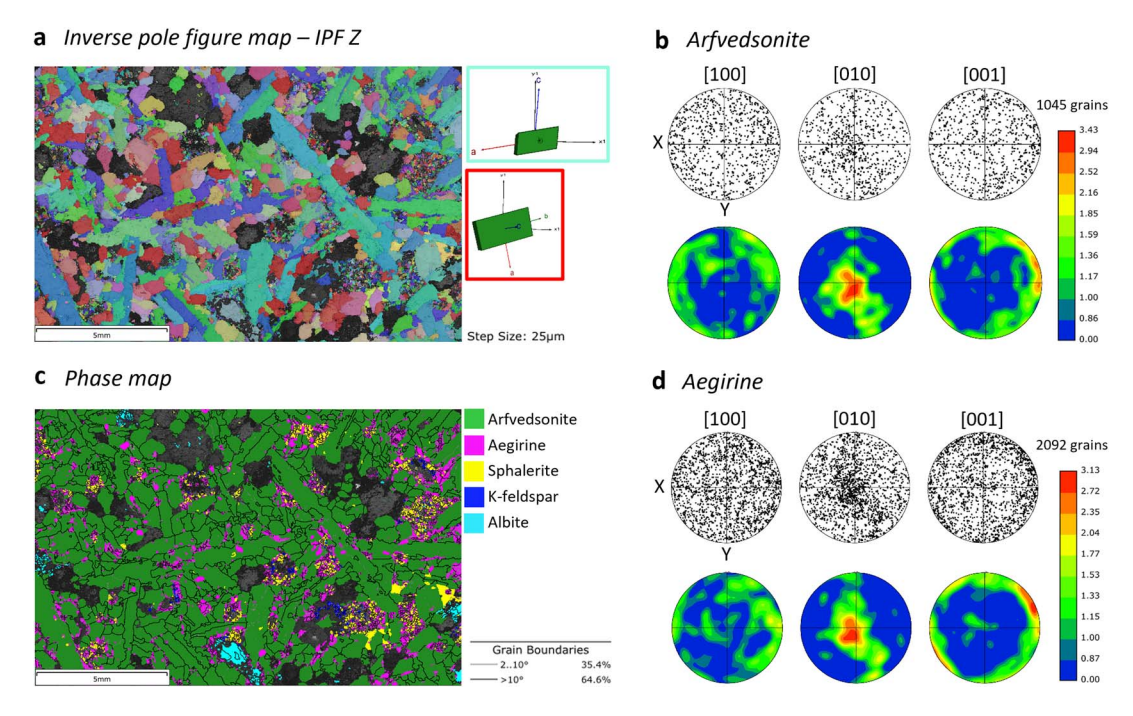


Fig. 13. (a) Inverse pole figure (IPF) map with respect to the Z direction (page normal) for arfvedsonite in ML-36. Schematic unit cells in the small light blue and red rectangular boxes provide example orientations of light blue to green grains and red grains, respectively. (b) Scattered pole figure data (top) and density contour plot of pole figure data (bottom) for arfvedsonite. (c) Phase map for kakortokite sample ML-36: green, arfvedsonite; pink, aegirine; blue, alkali feldspar; yellow, sphalerite; and light blue, albite. All grain boundaries in arfvedsonite are high-angle boundaries (>10°). (d) Scattered pole figure data (top) and density contour plot of pole figure data (bottom) for aegirine. For both contour plots, half width is 20° and data clustering is 10°. The color scales beside the pole figure contour plots illustrate multiples of uniform density (MUD) values.

that hornblende-rich amphibolites from Møre-Trøndelag Fault Complex (Central Norway) had K_3 perpendicular to the silicate foliation, but K_1 at a high angle to the visible lineation.

Several processes operating at different length-scales have been held responsible for intermediate magnetic fabrics in igneous rocks, including grain distributions, mixtures of different magnetic mineral phases present in the rock, and interactions among the ensemble of mineral grain magnetic moments (e.g., Rochette & Fillion 1988, Ferré 2002). Briefly, these processes include the interplay between the AMS, the remanent magnetization (anisotropy of anhysteretic remanent magnetization), and the magnetic history (i.e., isothermal remanent magnetizations) where the remanent magnetization imposes a bias on the AMS fabric and modification to the domain structure such as alternating field demagnetization prior to AMS measurements. Distribution anisotropy may interfere with grain shape anisotropy due to dipolar interactions between neighboring grains, and mixing of normal and inverse fabrics where the net susceptibility is carried by two or more magnetic mineral phases can produce composite or intermediate fabrics (Hargraves *et al.* 1991, Rochette *et al.* 1992).

In terms of paramagnetic minerals that yield intermediate fabrics, much remains unknown. For example, Hrouda (1982) states that chain silicates such as pyroxenes and amphiboles yield normal magnetic fabrics. Yet the early unpublished work of G.R. Parry (see Owens & Bamford 1976) contradicts Hrouda (1982), as several silicates show K₂ axes parallel to the long crystallographic axis (e.g., orthopyroxenes and riebeckite, as well as the nesosilicate staurolite (Wiedenmann et al. 1986, Rochette et al. 1992). Borg & Borg (1980) reported that the magnetic moment for Fe³⁺ in the solid solution series between riebeckite and arfvedsonite is not parallel to a principal crystallographic axis, leading to a magnetic anisotropy at an angle to the silicate mineral fabric. A detailed study of two clinopyroxene crystals (one magnesian hedenbergite and one aegirine-augite) shows the K₁ axis within the a-c crystallographic plane is oriented between the a and c directions (Baum et al. 1997). The b axis is close to the

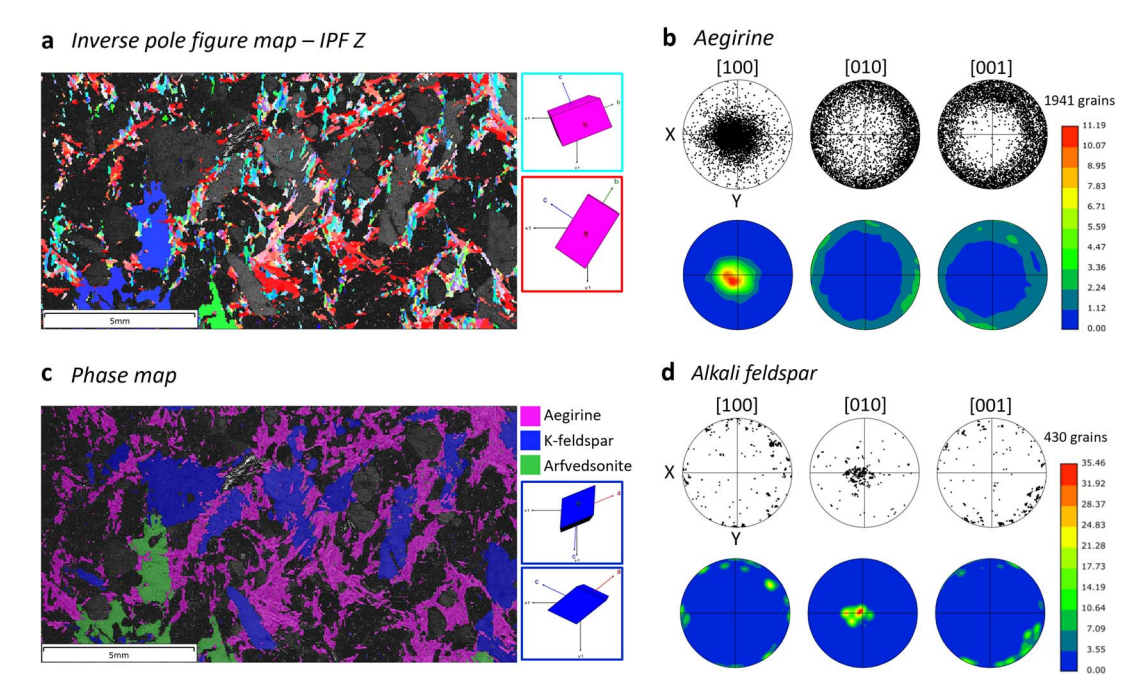


Fig. 14. (a) Inverse pole figure (IPF) map with respect to the Z direction (page normal) for aegirine in BR-1. Schematic unit cells in the small light blue and red rectangular boxes provide example orientations of light blue to green grains and red grains, respectively. An arfvedsonite oikocryst is visible on the left. (b) Scattered pole figure data (top) and density contour plot of pole figure data (bottom) for aegirine. (c) Phase map for lujavrite sample BR-1: pink, aegirine; blue, alkali feldspar; green, arfvedsonite; dark gray, eudialyte. (d) Scattered pole figure data (top) and density contour plot of pole figure data (bottom) for alkali feldspar. For both contour plots half width is 20° and data clustering is 10°. The color scales beside the pole figure contour plots illustrate multiples of uniform density (MUD) values.

K₂ and K₃ axes in the hedenbergite and the aegirine, respectively. A more recent set of studies by Biedermann et al. (2015a, b, 2018) characterized the magnetic fabrics of single crystals of a number of pyroxene and amphibole phases. For example, in the diopside-augite series, K2 is parallel to the b axis and K_1 is at $\sim 45^{\circ}$ to the c axis. Of direct relevance to the current study, Biedermann et al. (2015a) showed that single aegirine crystals have K2 parallel to b, with K₁ parallel to c. Biedermann et al. (2015b) reported intermediate fabrics for a range of amphibole species (tremolite, actinolite, and hornblende), with K₃ parallel to the crystallographic a axis and K₁ parallel to b, for measurements on single crystals. The latter study also showed that gedrite, an orthoamphibole, displayed normal magnetic fabrics. Richterite was shown to have K₂ parallel to b and K₁-K₃ distributed in the a-c plane. Biedermann et al. (2015a, b, 2018) attributed the variations in single amphibole crystal magnetic anisotropy to crystal structure, mineral chemical variations, the oxidation state of Fe, if present, and the presence or absence of Fe-oxide inclusions. We are in accord with the conclusion that the different results for amphiboles reported by Biedermann et al. and other authors (op. cit.) are at least partly a function of the complex variations in crystal chemistry observed in members of the amphibole group.

The rock magnetic data reported in the present study are interpreted to indicate that the remanence and susceptibility, and therefore the AMS fabrics, of the Ilímaussag kakortokites and lujavrites are dominated by a paramagnetic mineral phase (or phases). There is no evidence for a control on AMS fabrics by ferro/ferrimagnetic phases, consistent with petrographic observations on these rocks. The experimental results are consistent with the petrographic observations, which do not reveal the presence of any oxide phases in the samples examined. The morphology of eudialyte is equant in these samples, so this mineral's shape anisotropy is unlikely to be a significant contributor to the magnetic fabrics observed. We calculated the theoretical paramagnetic susceptibility for arfvedsonite using the formula of Syono (1960) and Rochette et al. (1992) together with the mineral chemical data of Lindhuber et al. (2015), and attained susceptibilities on the same order of magnitude as those reported in Table 1. Together with the relationship shown in Figure 4a, showing the positive correlation between K_{mean} and arfvedsonite modal proportions, we argue that the bulk

magnetic susceptibilities and hence the AMS fabrics in the kakortokites are controlled by arfvedsonite.

It is not uncommon for igneous rocks that lack ferro/ ferrimagnetic minerals to possess strong AMS fabrics (Bouchez 1997). That most kakortokite samples analyzed yield inverse AMS fabrics when compared to the welldeveloped arfvedsonite lamination, the latter clearly evident from our petrographic observations and EBSD data (Figs. 2, 14), is unusual. Notably, these fabrics clearly bear a resemblance to the inverse magnetic fabrics reported from some tourmaline-rich granites (e.g., Rochette 1988, Scaillet et al. 1990, Rochette et al. 1992), particularly samples ML-36, ML-37, ML54, and ML-58. Samples ML-35 and ML-40 exhibit neither ideal normal nor inverse fabrics. However, K₁ plunges relatively steeply, so it is suggested that these data represent a composite fabric, with the tensor for each averaging the arfvedsonite inverse fabric and another component. It is noteworthy in this regard that Lindhuber et al. (2015) reported some laminated kakortokites at the transition from black to white layers that preserve two shape preferred orientations of their alkali feldspar: one parallel or subparallel to layering and one dipping downward within layers. Lindhuber et al. (2015) did not speculate on the origin of this alkali feldspar fabric, but we observe such a configuration expressed by arfvedsonite in ML-35, ML-40, and ML-36. Note that for ML-36, this fabric can be observed in Figure 13a, where the red colored grains indicate that some arfvedsonite c axes are oriented parallel to the lamination normal.

The laminated lujavrites (BR-1 and BR-9) do not exhibit perfectly normal nor inverse fabrics. The AMS ellipsoid shapes in BR-1 and BR-9 are both relatively strongly oblate, but there is strong discordance between K_3 and the pole to the visible lamination (>60° in both). The linear and planar elements of the AMS in both samples are approximately equal. The bulk magnetic susceptibilities for the lujavrites also appear to correlate with the differences in arfvedosonite abundance (Fig. 4a, Table 1). It is possible that aggirine, which is the main carrier phase for the mineral lamination in both BR-1 and BR-9 and which should have a normal magnetic fabric (Biedermann et al. 2015a), exerts a partial control on the AMS fabric. However, we suggest that the deviation from normal fabrics for these samples is explained by the presence of arfvedsonite, which has an order of magnitude higher magnetic susceptibility and which is not strongly aligned, in all samples (Fig. 4a). This is supported by the EBSD data for BR-1, which indicate that the distribution of aegirine within the foliation planes produces a strong (crystallographically controlled) mineral lamination (Fig. 14a, b). We calculated theoretical bulk susceptibilities for aegirine based on the mineral chemical data reported in Ratschbacher et al. (2015) and produced values on the order of $50-80 \times 10^{-6}$ SI, an order of magnitude lower than that calculated for arfvedsonite. This suggests that the AMS fabrics in the lujavrites are largely, if not completely, controlled by the lower abundance, higher susceptibility phase, with a contribution from the higher abundance, lower susceptibility phase (aegirine), to give a mixed fabric result and explaining the lack of a clear relationship between the mineral lamination and the magnetic fabric. The EBSD data also suggest that the anastomosing nature of aegirine crystals within the rock does not significantly affect the bulk fabric. In BR-1, the sparse occurrence of large arfvedsonite oikocrysts means that any measurements of this mineral's CPO are not statistically significant and are therefore of limited value for our interpretations. In BR-22, finegrained arfvedsonite is disseminated throughout the sample, up to 15 vol.%, but an insufficient number of sub-samples were analyzed to fully interpret the AMS fabrics.

Finally, although several sulfide phases have been reported in the Ilímaussaq kakortokites and lujavrites (e.g., Lindhuber et al. 2015, Ratschbacher et al. 2015), supported by the petrographic observations reported here, these are not considered to be significant contributors to the AMS. The principal reason for this is that they exist in trace amounts and similar AMS fabrics are present in a range of samples whether or not the sulfide is observed. Given the strong, albeit inverse, relationship observed between some of the kakortokite AMS fabrics and the silicate lamination, it is not considered likely that isolated, anhedral irregularly oriented and trace amounts of sulfide can explain the magnetic fabrics observed. Furthermore, the hysteresis curves presented here show a convincing paramagnetic response to the applied field up to 3.0 Tesla (Fig. 10), suggesting that ferrimagnetic sulfide (e.g., pyrrhotite) is not significant in carrying the AMS fabrics.

Mechanisms of fabric acquisition in the Ilímaussaq cumulates

Mineral lamination in the kakortokites and lujavrites of the Ilímaussaq intrusion has generally been interpreted in the context of layer-forming processes; however, there remains no generally accepted model for the formation of either (see Upton et al. 1996 and Marks & Markl 2015 for comprehensive reviews). Models for the rhythmic layering of the kakortokites have notably included density-driven segregation of the mafic crystals from the felsic ones during settling (e.g., Bohse et al. 1971, Ferguson 1964, Ussing 1912), in situ crystallization following suppression of feldspar growth (Larsen & Sørensen 1987), and crystal mat formation (Bons et al. 2015, Lindhuber et al. 2015). The acicular habit of arfvedsonite and its settling to form dense crystal mats that then acted as local

barriers to settling and flotation were envisaged as factors in the development of the black, red, and white kakortokites by Lindhuber *et al.* (2015). However, Hunt *et al.* (2017) adapted the model of Larsen & Sørensen (1987) and proposed *in situ* crystallization of the black and red portions of the kakortokite layers, with delayed crystallization of feldspar and subsequent localized sorting, *i.e.*, settling and flotation, to produce each of the rhythmic kakortokite layers.

The long-standing model for lujavrite formation envisages them as having crystallized in situ, sandwiched between older (roof series) rocks above them and the related but earlier crystallized kakortokites that lie stratigraphically beneath them (Larsen & Sørensen 1987). However, this model was challenged by Ratschbacher et al. (2015), who interpreted the lujavrite sequence as a distinct late-stage intrusive unit that forms a sill-like structure. They interpreted the lamination observed in the lujavrites as magmatic in origin and noted, as observed here, that foliations wrap phenocrysts but are also locally overgrown by the rims of such phenocrysts, demonstrating the presence of melt in interstitial spaces during fabric formation. Ratschbacher et al. (2015) documented the presence of a lineation carried by aegirine in lujavrites lower in the sequence, including BR-1. They also reported that intra-crystal (plastic) deformation microstructures are comparatively rare, though they suggested that fabric-forming processes continued into the postcumulus and perhaps even the subsolidus stage, based on the presence of late-crystallizing phases (e.g., analcime) in pressure shadows and minor undulose extinction in late-stage interstitial minerals.

Our new AMS data do not allow for direct interpretations to be made with respect to kakortokite and lujavrite petrogenesis, but combining the observations from the magnetic fabrics with those from the EBSD data and petrography reveals interesting insights. Allowing for the inverse fabrics in most of the kakortokites, K3 should thus reflect a mineral lineation. The AMS data show that K₃ is weakly defined, if resolvable at all, compared to K_1 , in the kakortokites. This observation, together with the arfvedsonite EBSD data for ML-36 (Fig. 13), indicating a decussate texture, suggests that the kakortokites do not contain a lineation that can be related to flow. Mechanisms of fabric acquisition that can develop planar fabrics with no lineation in layered intrusion cumulates could be primary, such as crystal settling, or postcumulus, such as compaction. Other processes, such as either deposition from within localized (crystal-rich) density currents or asymmetric shearing of the partly solidified crystal mush, might be expected to produce a silicate lineation. Holness et al. (2017b) set out a range of microstructural criteria by which solid-state deformation (e.g., compaction) of cumulates could be discerned, although they did not explicitly consider the case where late-stage postcumulus processes operate on already laminated cumulate, accentuating or complicating an already existing fabric. Notwithstanding, evidence for viscous deformation is an important criterion on which to base interpretations of compaction (Holness et al. 2017b). The main fabric-forming minerals in the kakortokites, arfvedsonite and alkali feldspar, have undergone a degree of secondary postcumulus alteration in most of the samples studied here, but show only localized and minor evidence for brittle deformation, such as intra-crystal fractures and bending of euhedral crystals. Other microstructural evidence of solid-state deformation (such as twin dislocations in feldspar) or dynamic recrystallization are rare to absent. This observation is in agreement with Lindhuber et al. (2015), who found that evidence for solid-state deformation of the high aspect ratio cumulus phases such as alkali feldspar was relatively rare.

A primary mode for fabric formation thus seems most likely for the kakortokites. Hunt et al. (2017) argued that because the black kakortokites exhibit a stronger lamination than the white kakortokites, compaction must have played a role in enhancing (accentuating) the fabric in the former. However, based on the criteria set out by Holness et al. (2017b), we argue that compaction must have been relatively limited, because of the lack of microstructural evidence observed for solid-state deformation. A model where formation of each of the rhythmic kakortokite layers initially involved development of dense mats of arfvedsonite explains our observations better. For example, such arfvedsonite mats would be relatively impermeable, meaning that some interstitial melt could be trapped to react with primocrysts in the crystal mush, explaining why the cumulus phases (e.g., alkali feldspar and arfvedsonite) in the black kakortokites are generally more altered than in the white kakortokite. In this light, it is worth noting that the EBSD data suggest topotactic growth of aegirine on the edges of arfvedsonite crystals (Fig. 13c). Arfvedsonite in the white kakortokites exhibits magnetic foliations similar, albeit weaker, to those in the black kakortokites, which can be accounted for in the crystal mat model by localized flotation of alkali feldspar-rich cumulate. Samples ML-36 and ML-37 come from the folded outcrop of Lindhuber et al. (2015) shown in Figure 2h, and it is notable that they have the best defined magnetic lineations (K₃), although it is difficult to speculate further on the origin of the folding on this basis because our new EBSD data do not reveal the presence of a lineation in the arfvedsonite population in ML-36. Nonetheless, the presence of this folding within the kakortokites suggests that localized 'soft sediment' deformation may have occurred. However, it should be noted that the field evidence for postcumulus deformation, such as folding in the kakortokites, occurs only very locally and other sedimentary structures, such as trough banding and current

bedding, are mainly confined to the intrusion margins or occur close to large autoliths enclosed in the kakortokite sequences (Upton & Pulvertaft 1961, Bohse *et al.* 1971).

The lujavrite petrofabric in BR-1 bears some similarities to schistosity in metamorphic rocks, with the arfvedsonite oikocrysts and eudialyte phenocrysts resembling 'porphyroblasts' that have evidently been rotated with respect to the foliation (evidenced by the orientation of the tablet-shaped chadacrysts in the arfvedsonite) and with the aegirine typically wrapping these objects, creating pressure shadows within the lamination plane, particularly adjacent to eudialyte crystals. The orientation of the alkali feldspar inclusions in the arfvedsonite oikocryst appears to be continuous with the lamination outside the oikocryst, carried by aegirine and alkali feldspar. According to typical interpretations of such inclusion trail textures in metamorphic rocks (Schoneveld 1977, Vernon 2004), this signifies rotation of the oikocryst during formation of the aegirine petrofabric. These observations point to fabric acquisition at the postcumulus stage, rather than crystal settling or deposition from density currents. Although the lujavrite AMS data suggest the presence of a magnetic lineation (K1) in the samples, the EBSD data show that aggirine carries a cross-lineation of c axes defining a decussate texture, and thus does not preserve any convincing evidence for flow-related or metamorphic-like processes. Thus, the aegirine fabric is principally planar. The observation from the EBSD data that the aegirine a axis grows subparallel to the alkali feldspar b axis suggests a topotactic relationship between these two phases. Given that aegirine needles also crosscut the boundaries of eudialyte phenocrysts, it appears that aggirine is a relatively latecrystallizing phase in this rock. This conclusion fits with the interpretation of Ratschbacher et al. (2015), that much of the lujavrite texture was being heavily modified into the postcumulus stage, possibly as a result of dissolution-reprecipitation. Our new data thus offer no reason to argue against their conclusion that the lujavrite is a syn-magmatic intrusive unit, and indeed offer indirect support to that interpretation. Further work will be required to decipher the precise controls on aggirine nucleation and growth in this context, but our observations that the aegirine fabric may mimic a preexisting feldspar lamination offers a potentially useful starting point for such investigations.

With respect to mineralization in the Ilimaussaq Complex, eudialyte-group primocrysts are a major host for the REE in the kakortokites and the lujavrites. The textural evidence from kakortokites and lujavrites reported here and by Ratschbacher *et al.* (2015), Borst *et al.* (2018), and Marks *et al.* (2020) points to protracted crystallization of eudialyte into the postcumulus stage, since aegirine needles crosscut the edges of

eudialyte phenocrysts. The outer rims of compositionally zoned eudialytes in lujavrites are locally highly enriched in REE+Y (Ratschbacher *et al.* 2015), perhaps implying that fractionated interstitial melts migrating within the crystal mush had the most 'mineralizing potential'. Eudialyte in the kakortokites also exhibits compositionally distinct postcumulus outer rims (Marks *et al.* 2020). In the lujavrites, our EBSD data suggest a clustering of eudialyte c axes perpendicular to the mineral lamination planes which, when combined with the suggestion of topotactic growth of at least some aegirine onto alkali feldspar, indicates that a planar arrangement of minerals was present at the crystal mush stage and was potentially able to control interstitial melt movement and secondary mineral growth.

Conclusions

This study presents AMS and rock magnetic data from highly evolved nepheline syenites (kakortokites and lujavrites) of the Ilímaussaq intrusion to gain further insight into the mechanisms of formation of the silicate petrofabric in these cumulate rocks. The magnetic fabrics observed are complex and do not directly reflect the silicate petrofabric, which is carried predominantly by arfvedsonite plus alkali feldspar in the kakortokites and mainly by aegirine in the lujavrites. Instead, the data show inverse fabrics for the kakortokites and composite fabrics in the lujavrites. Our comprehensive suite of rock magnetic experiments support the petrographic observations that there are no Fe-Ti-oxide minerals present in the samples studied. The rocks are therefore dominated by paramagnetic behavior. This implies that the inverse magnetic fabrics recorded in the kakortokites studied result from a mineralogical effect, in a manner similar to that exhibited by tourmaline in certain granite intrusions. Based on the control arfvedsonite evidently exerts on bulk magnetic susceptibilities in these rocks, this phase is the likely candidate. The composite fabrics in the lujavrites are a consequence of a mixed response between the relatively low magnetic susceptibility aegirine, which defines the silicate petrofabric, and the relatively high susceptibility arfvedsonite, which is present in lower modal abundances than aegirine and does not, on the basis of petrographic observation, contribute to the mineral lamination. Our results also allow for some indirect inferences to be made on fabric acquisition. The lack of a single resolvable silicate lineation and the relative weakness of the linear component of the AMS fabrics indicates that the kakortokites and lujavrites contain dominantly planar fabrics. For the kakortokites, the data appear to best support the crystal mats model. The new data produced for the lujavrites align reasonably well with the interpretation of an intrusive origin, such that much of their microstructural character was imposed at the postcumulus stage. This study highlights the powerful utility of combining EBSD with the AMS technique in deciphering the processes responsible for mineral alignment in igneous cumulates.

ACKNOWLEDGMENTS

BO'D is grateful to Brian Upton for sharing insights into the petrology of the Ilímaussaq cumulate rocks. BO'D acknowledges research support from the Natural Sciences and Engineering Research Council of Canada (NSERC Discovery Grant) and from the Newmont Chair in Economic Geology (University of Ottawa). MSP acknowledges partial support from the National Science Foundation Grant DMR-2122108 (PREM) for the rock magnetic analysis. EM would like to acknowledge the Liverpool Earth Science EBSD-SEM laboratory, now part of the Scanning Electron Microscopy Shared Research Facility (SEM SRF) at the University of Liverpool, for supporting all EBSD analyses presented in this study. Olivier Bolle and two anonymous reviewers are thanked for detailed comments on an earlier version of this manuscript. Ole Skursch and James Scoates are thanked for their constructive reviews of this iteration.

REFERENCES

- ANDERSEN, S., BOHSE, H., & STEENFELT, A. (1981) A geological section through the southern part of the Ilímaussaq intrusion. *Rapport Grønlands Geologiske Undersøgelse* 103, 39–42.
- BAILEY, J.C., GWOZDZ, R., ROSE-HANSEN, J., & SØRENSEN, H. (2001) Geochemical overview of the Ilimaussaq alkaline complex, South Greenland. Geology of Greenland Survey Bulletin 190, 35–53.
- BAUM, E., TREUTMAN, W., LOTTERMOSER, W., & AMTHAUER, G. (1997) Magnetic properties of the clinopyroxenes aegirine and hedenbergite: A magnetic susceptibility study on single crystals. *Physics and Chemistry of Minerals* 24, 294–300.
- BIEDERMANN, A.R., PETTKE, T., KOCH, C.B., & HIRT, A.M. (2015a) Magnetic anisotropy in clinopyroxene and orthopyroxene single crystals. *Journal of Geophysical Research Solid Earth* 120, JB011678.
- BIEDERMANN, A.R., PETTKE, T., KOCH, C.B., & HIRT, A.M. (2015b) Magnetic anisotropy in natural amphibole crystals. *American Mineralogist* 100(8–9), 1940–1951.
- BIEDERMANN, A.R., KUNZE, K., & HIRT, A.M. (2018) Interpreting magnetic fabrics in amphibole-bearing rocks. *Tectonophysics* 722, 566–576.
- BOHSE, H. & ANDERSEN, S. (1981) Review of the stratigraphic divisions of the kakortokite and lujavrite in southern Ilímaussaq. Rapport Grønlands Geologiske Undersøgelse 103, 53–62.

- BOHSE, H., BROOKS, C.K., & KUNZENDORF, H. (1971) Field observations on the Kakortokites of the Ilímaussaq intrusion, South Greenland, including mapping and analyses by portable X-ray fluorescence equipment for zirconium and niobium. Rapport Grønlands Geologiske Undersøgelse 38, 5–43.
- Bons, P.D., Baur, A., Elburg, M.E., Lindhuber, M.J., Marks, M.A.W., Soesoo, A., Van Miligen, B.O., & Walte, N.P. (2015) Layered intrusions and traffic jams. *Geology* 43, 71–74.
- BORG, R.J. & BORG, I.Y. (1980) Mössbauer study of behavior oriented single crystals of riebeckite at low temperatures and their magnetic properties. *Physics and Chemistry of Minerals* 5, 219–234.
- BORRADAILE, G.J. & JACKSON, M. (2004) Anisotropy of magnetic susceptibility (AMS): Magnetic petrofabrics of deformed rocks. Geological Society Special Publication 238, 299–360.
- Borradaile, G.J. & Jackson, M. (2010) Structural geology, petrofabrics and magnetic fabrics (AMS, AARM, AIRM). *Journal of Structural Geology* **32**(10), 1519–1551.
- Borradaile, G.J. & Puumala, M.A. (1989) Synthetic magnetic fabric in plasticene. *Tectonophysics* **164**, 73–78.
- BORST, A.M., FRIS, H., NIELSEN, T.F.D., & WAIGHT, T.E. (2018) Bulk and mush melt evolution in agpaitic intrusions: Insights from compositional zoning in eudialyte, Ilimaussaq Complex, South Greenland. *Journal of Petrology* 59(4), 589–612.
- BOUCHEZ, J.L. (1997) Granite is never isotropic: An introduction to AMS studies of granitic rocks. *In* Granite: From Segregation of Melt to Emplacement Fabrics (J.L. Bouchez, D.H.W. Hutton, & W.E. Stephens, eds.). Kluwer, Dordrecht, Netherlands (95–112).
- Boudreau, A. (1999) Fluid fluxing of cumulates: The J-M Reef and associated rocks of the Stillwater Complex, Montana. *Journal of Petrology* **40**, 755–772.
- Cheadle, M.J. & Gee, J.S. (2017) Quantitative textural insights into the formation of gabbro in mafic intrusions. *Elements* **13**(6), 409–414.
- CRUDEN, A.R. & LAUNEAU, P. (1994) Structure, magnetic fabric and emplacement of the Archean Lebel Stock, SW Abitibi Greenstone Belt. *Journal of Structural Geology* 16(5), 677–691.
- DE WALL, H. (2000) The field dependence of AC susceptibility in titanomagnetites: Implications for the anisotropy of magnetic susceptibility. *Geophysical Research Letters* 27(16), 2409–2411.
- DUNLOP, D.J. & ÖZDEMIR, O. (1997) Rock Magnetism, Fundamentals and Frontiers. Cambridge University Press, Cambridge, UK, 573 pp.
- ELLWOOD, B.B., BALSAM, W., BURKART, B., LONG, G., & BUHL, M. (1986) Anomalous properties in rocks containing the mineral siderite: Paleomagnetic implications. *Journal of Geophysical Research* 91, 12779–12790.

- FERGUSON, J. (1964) Geology of the Ilimaussaq alkaline intrusion, South Greenland. Bulletin Grønlands Geologiske Undersøgelse 39, 1–82.
- FERRÉ, E.C (2002) Theoretical models of intermediate and inverse AMS fabrics. *Geophysical Research Letters* **29**(7), 1–31.
- FERRÉ, E.C. & AMÉGLIO, L. (2000) Preserved magnetic fabrics vs annealed microstructures in the syntectonic recrystallised George granite, South Africa. *Journal of Structural Geology* 22, 1199–1219.
- GIANALELLA, P.R. & HELLER, F. (1994) Rock magnetism of deformed upper Triassic limestones for the Lagonegro Basin (Southern Apennines, Italy). *Geophysical Research Letters* 21, 2665–2668.
- HANLEY, J.J., MUNGALL, J.E., PETTKE, T., SPOONER, E.T.C., & BRAY, C.J. (2008) Fluid and halide melt inclusions of magmatic origin in the Ultramafic and Lower Banded Series, Stillwater Complex, Montana, USA. *Journal of Petrology* 49(6), 1133–1160.
- HARGRAVES, R.B., CHAN, C.Y., & JOHNSON, D. (1991) Distribution anisotropy: The cause of AMS in igneous rocks? Geophysical Research Letters 18, 2193–2196.
- HEPWORTH, L.N., DALY, J.S., GERTISSER, R., JOHNSON, C.G., EMELEUS, C.H., & O'DRISCOLL, B. (2020) Rapid crystallization of precious-metal-mineralized layers in mafic magmatic systems. *Nature Geoscience* 13(5), 375–381.
- HIRT, A. & GEHRING, A. (1991) Thermal alteration of the magnetic mineralogy in ferruginous rocks. *Journal of Geophysical Research* 96, 9947–9954.
- Holness, M.B., Sides, R., Prior, D.J., Cheadle, M.J., & Upton, B.G.J. (2012) The peridotite plugs of Rum: Crystal settling and fabric development in magma conduits. *Lithos* **134–135**, 23–40.
- HOLNESS, M.B., NIELSEN, T.F., & TEGNER, C. (2017a) The Skaergaard intrusion of East Greenland: Paradigms, problems and new perspectives. *Elements* 13(6), 391–396.
- HOLNESS, M.B., VUKMANOVIC, Z., & MARIANI, E. (2017b) Assessing the role of compaction in the formation of adcumulates: A microstructural perspective. *Journal of Petrology* 58, 643–674.
- HOPKINSON, J. (1890) Magnetic properties of alloys of nickel and iron. Proceedings of the Royal Society of London 48, 1–13.
- HROUDA, F. (1982) Magnetic anisotropy of rocks and its application in geology and geophysics. *Geophysical Surveys* 5, 37–82.
- HROUDA, F. (2003) Indices for numerical characterization of the alteration processes of magnetic minerals taking place during investigation of temperature variation of magnetic susceptibility. Studia Geophysica et Geodaetica 47, 847–861.
- HUNT, E.J., FINCH, A.A., & DONALDSON, C.H. (2017) Layering in peralkaline magmas, Ilímaussaq Complex, S Greenland. *Lithos* 268–271, 1–15.

- IHMLÉ, P.F., HIRT, A., LOWRIE, W., & DIETRICH, D. (1989) Inverse magnetic fabric in deformed limestones of the Morcles nappe, Switzerland. *Geophysical Research Letters* 16, 1383–1386.
- IRVINE, T.N., ANDERSON, J.C., & BROOKS, C.K. (1998) Included blocks (and blocks within blocks) in the Skaergaard intrusion: Geologic relations and the origins of rhythmic modally graded layers. *Geological Society of America Bulletin* 110, 1398–1447.
- IRVING, E. (1970) The Mid-Atlantic Ridge at 45N, XIV, Oxidation and magnetic properties of basalts: Review and discussion. Canadian Journal of Earth Sciences 7, 1528–1583.
- JACKSON, M. (1991) Anisotropy of magnetic remanence: A brief review of mineralogical sources, physical origins and geological applications. *Pure and Applied Geophysics*, 136, 1–28.
- JELINEK, V. (1978) Statistical processing of anisotropy of magnetic susceptibility measured on groups of specimens. Studia Geophysica et Geodaetica 22, 50–62.
- JELÍNEK, V. (1981) Characterization of the magnetic fabric of rocks. *Tectonophysics* 79(3–4), T63–T67.
- JOHNSON, H.P. & ATWATER, T. (1977) A magnetic study of basalts from the mid-Atlantic ridge at 37°N. Geological Society of America Bulletin 88, 637–647.
- KHAN, M.A. (1962) The anisotropy of magnetic susceptibility of some igneous and metamorphic rocks. *Journal of Geophysical Research* 67, 2873–2885.
- KOOPMANS, L., McCARTHY, W., & MAGEE, C. (2022) Dyke architecture, mineral layering, and magmatic convection; new perspectives from the Younger Giant Dyke Complex, S. Greenland. *Geochemistry, Geophysics, Geosystems* 23(3), e2021GC010260.
- KRUMREI, T.V., VILLA, I.M., MARKS, M.A.W., & MARKL, G. (2006) A ⁴⁰Ar/³⁹Ar and U/Pb isotopic study of the Ilímaussaq complex, South Greenland: Implications for the ⁴⁰K decay constant and for the duration of magmatic activity in a peralkaline complex. *Chemical Geology* 227, 258–273.
- LARSEN, L.M. & SØRENSEN, H. (1987) The Ilímaussaq intrusion-progressive crystallization and formation of layering in an agnaitic magma. *In Alkaline Igneous Rocks.* (J.G. Fitton & B.G.J. Upton, eds.). *Geological Society of London Special Publications* 30, 473–488.
- LAUNEAU, P. & CRUDEN, A.R. (1998) Magmatic fabric acquisition mechanisms in a syenite: Results of a combined anisotropy of magnetic susceptibility and image analysis study. *Journal* of Geophysical Research 103, 5067–5089.
- LINDHUBER, M.J., MARKS, M.A.W., BONS, P.D., WENZEL, T., & MARKL, G. (2015) Crystal mat-formation as an igneous layering-forming process: Textural and geochemical evidence from the lower layered nepheline syenite sequence of the Ilímaussaq complex, South Greenland. *Lithos* 224–225, 295–309.

- MARIANI, E., PRIOR, D.J., COVEY-CRUMP, S.J., MECKLENBURGH, J., TATHAM, D., & WHEELER, J. (2009) Microstructure evolution during creep and annealing of minerals and rocks. *Microscopy* and Microanalysis 15, 412–413.
- MARKS, M.A.W. & MARKL, G. (2015) The Ilimaussaq alkaline complex, South Greenland: Current understanding and open questions. *In* Layered Intrusions (B. Charlier, O. Namur, R. Latypov, & C. Tegner, eds). Springer, Dordrecht, Netherlands (649–691).
- Marks, M.A.W. & Markl, G. (2017) A global review on agnaitic rocks. Earth Science Reviews 173, 229–258.
- MARKS, M.A.W., VENNEMAN, T.W., SIEBEL, W., & MARKL, G. (2004) Nd-, O-, and H-isotopic evidence for complex, closed-system fluid evolution of the peralkaline Ilímaussaq intrusions, South Greenland. *Geochimica et Cosmochimica* Acta 68, 3379–3395.
- MARKS, M.A.W., HETTMAN, K., SCHLLING, J., FROST, B.R., & MARKL, G. (2011) The mineralogical diversity of alkaline igneous rocks: Critical factors for the transition from miaskitic to agpaitic phase assemblages. *Journal of Petrology* 52, 439–455.
- MARKS, M.A.W., EGGENKAMP, H.G.M., ATANASOVA, P., MUNDEL, F., KÜMMEL, S., HAGEN, M., WENZEL, T., & MARKL, G. (2020) Review on the compositional variation of eudialyte-group minerals in the Ilimaussaq Complex (South Greenland). *Minerals* 10, 1011.
- MARSHALL, M. & Cox, A. (1972) Magnetic changes in pillow basalts due to seafloor weathering. *Journal of Geophysical Research* 77, 6459–6469.
- McBirney, A.R. & Nicolas, A. (1997) The Skaergaard Layered Series: Part II. Dynamic layering. *Journal of Petrology* 38, 569–580.
- McBirney, A.R. & Noyes, R.M. (1979) Crystallization and layering in the Skaergaard intrusion. *Journal of Petrology* 20, 487–554.
- MEURER, W.P. & BOUDREAU, A.E. (1998a) Compaction of igneous cumulates part I: Geochemical consequences for cumulates and liquid fractionation trends. *The Journal of Geology* 106(3), 281–292.
- MEURER, W.P. & BOUDREAU, A.E. (1998b) Compaction of igneous cumulates part II: Compaction and the development of igneous foliation. *The Journal of Geology* 106(3), 293–304.
- Moskowitz, B.M. (1981) Methods of estimating Curie temperatures of titanomagnetites from experimental Js-T data. *Earth and Planetary Science Letters* **53**, 84–88.
- NISHITANI, T. & KONO, M. (1983) Curie temperature and lattice constant of oxidized titanomagnetite. *Geophysical Journal International* 74, 585–600.
- O'Driscoll, B., Hargraves, R.B., Emeleus, C.H., Troll, V. R., Donaldson, C.H., & Reavy, R.J. (2007) Magmatic

- lineations inferred from anisotropy of magnetic susceptibility fabrics in Units 8, 9, and 10 of the Rum Eastern Layered Series, NW Scotland. *Lithos* **98**(1–4), 27–44.
- O'DRISCOLL, B., STEVENSON, C.T.E., & TROLL, V.R. (2008) Mineral lamination development in layered gabbros of the British Palaeogene Igneous Province: A combined anisotropy of magnetic susceptibility, quantitative textural and mineral chemistry study. *Journal of Petrology* 49(6), 1187–1221.
- O'DRISCOLL, B., FERRÉ, E.C., STEVENSON, C.T.E., & MAGEE, C. (2015) The significance of magnetic fabrics in layered mafic-ultramafic intrusions. *In* Layered Intrusions (B. Charlier, O. Namur., R. Latypov, & C. Tegner, eds). Springer, Dordrecht, Netherlands (295–329).
- OWENS, W.H. (1974) Mathematical model studies on factors affecting the magnetic anisotropy of deformed rocks. *Tec*tonophysics 24, 115–131.
- OWENS, W.H. (1994) Laboratory drilling of field-orientated block samples. *Journal of Structural Geology* 16, 1719–1721.
- OWENS, W.H. (2000) Statistical analysis of normalised and unnormalised second-rank tensor data, with application to measurements of anisotropy of magnetic susceptibility. *Geophysical Research Letters* 27, 2985–2988.
- OWENS, W.H. & BAMFORD, D. (1976) Magnetic, seismic and other anisotropic properties of rock fabrics. *Philosophical Transactions of the Royal Society London* A283, 55–68.
- PARÉS, J.M. (2004) How deformed are weakly deformed mudrocks? Insights from magnetic anisotropy. *In Magnetic Fabrics*: Methods and Applications (F. Martin-Hernandez, C. Aubourg, & M. Jackson, eds). Geological Society of London Special Publications 238, 191–203.
- PARÉS, J.M. & VAN DER PLUIJM, B.A. (2002) Evaluating magnetic lineations (AMS) in deformed rocks. *Tectonophysics* 350, 283–298.
- Parsons, I. (2012) Full stop for mother Earth. *Elements* 8, 396–398.
- Petford, N. (2009) Which effective viscosity? *The Mineral*ogical Magazine **73**(2), 167–191.
- PETRONIS, M.S., O'DRISCOLL, B., & LINDLINE, J. (2011) Late stage oxide growth associated with hydrothermal alteration of the Western Granite, Isle of Rum, NW Scotland. Geochemistry, Geophysics, Geosystems 12, e2010GC003246.
- PFAFF, K., KRUMREI, T.V., MARKS, M.A.W., WENZEL, T., RUDOLF, T., & MARKL, G. (2008) Chemical and physical evolution of the 'lower layered series' from the nepheline syenitic Ilímaussaq intrusion, South Greenland: Implications for the origin of magmatic layering in peralkaline felsic liquids. *Lithos* 106, 280–296.
- POTTER, D.K. & STEPHENSON, A. (1988) Single-domain particles in rocks and magnetic fabric analysis. *Geophysical Research Letters* 15, 1097–1100.

- PRIOR, D.J., MARIANI, E., & WHEELER, J. (2009) EBSD in the Earth Sciences: Applications, common practice, and challenges. *In* Electron Backscatter Diffraction in Materials Science (A.J. Schwartz, M. Kumar, B.L. Adams, & D.P. Field, eds). New York: Springer (345–360).
- RATSCHBACHER, B.C., MARKS, M.A.W., BONS, P.D., WENZEL, T., & MARKL, G. (2015) Emplacement and geochemical evolution of highly evolved syenites investigated by a combined structural and geochemical field study: The lujavrites of the Ilímaussaq complex, SW Greenland. *Lithos* 231, 62–76.
- READMAN, P.W. & O'REILLY, W. (1972) Magnetic properties of oxidized (cation-deficient) titanomagnetites (Fe, Ti)₃O₄. *Journal of Geomagnetism & Geoelectricity* 24, 69–90.
- ROCHETTE, P. (1988) Inverse magnetic fabric in carbonate-bearing rocks. Earth & Planetary Science Letters 90, 229–237.
- ROCHETTE, P. & FILLION, G. (1988) Identification of multicomponent anisotropy in rocks using various field and temperature values in a cryogenic magnetometer. *Physics of the Earth and Planetary Interiors* **51**, 379–386.
- ROCHETTE, P., FILLION, G., MATTÉI, J.L., & DEKKERS, M. (1990) Magnetic transition at 30–34 Kelvin in pyrrhotite: Insight into a widespread occurrence of this mineral in rocks. *Earth and Planetary Science Letters* 98, 319–328.
- ROCHETTE, P., JACKSON, M., & AUBOURG, C. (1992) Rock magnetism and the interpretation of the anisotropy of magnetic susceptibility. *Reviews in Geophysics* **30**, 209–226.
- ROCHETTE, P., SCAILLET, B., GUILLOT, S., LE FORT, P., & PÊCHER, A. (1994) Magnetic properties of the High Himalayan leucogranites: Structural implications. *Earth & Planetary Science Letters* **126**, 217–234.
- ROCHETTE, P., AUBOURG, C., & PERRIN, M. (1999) Is this magnetic fabric normal? A review and case studies in volcanic formations. *Tectonophysics* **307**, 219–234.
- ROCHETTE, P., LORAND, J.-P., FILLION, G., & SAUTTER, V. (2001) Pyrrhotite and the remanent magnetization of SNC meteorites: A changing perspective of Martian magnetism. *Earth and Planetary Science Letters* **190**(1–2), 1–12.
- SCAILLET, B., FRANCE-LANORD, C., & LE FORT, P. (1990) Badrinath-Gangotri plutons (Garhwal, India): Petrological and geochemical evidence for fractionation processes in a high Himalayan leucogranite. *Journal of Volcanology and Geothermal Research* 44, 163–188.
- SCHONEVELD, C. (1977) A study of some typical inclusion patterns in strongly paracrystalline rotated garnets. *Tectonophysics* 39, 453–471
- SELKIN, P.A., GEE, J.S., & MEURER, W.P. (2014) Magnetic anisotropy as a tracer of crystal accumulation and transport, Middle Banded Series, Stillwater Complex, Montana. *Tectonophyics* 629, 123–137.

- SØRENSEN, H. (1997) The agpaitic rocks An overview. The Mineralogical Magazine 61, 485–498.
- SØRENSEN, H. (2001) Brief introduction to the geology of the Ilímaussaq alkaline complex, South Greenland, and its exploration history. Geology of Greenland Survey Bulletin 190, 7–23.
- SYONO, Y. (1960) Magnetic susceptibility of some rock forming silicate minerals such as amphiboles, biotites, cordierites and garnets. *Journal of Geomagnetism and Geoelectricity* 11, 85–93.
- Tarling, D.H. & Hrouda, F. (1993) *The Magnetic Anisotropy of Rocks*. Chapman and Hall, New York, USA, 217 pp.
- TAUXE, L. (1998) Paleomagnetic Principles and Practice (Modern Approaches in Geophysics 17). Kluwer Academic Publishers, Dordrecht, Netherlands, 301 pp.
- UPTON, B.G.J. & PULVERTAFT, T.C.R. (1961) Textural features of some contrasted igneous cumulates from South Greenland. *Meddelelser om Grønland* 123, 1–29.
- UPTON, B.G.J., PARSONS, I., EMELEUS, C.H., & HODSON, M.E. (1996) Layered alkaline igneous rocks of the Gardar Province, South Greenland. *In* Layered Intrusions (R.G. Cawthorn, ed.). Elsevier Science, Amsterdam (331–363).
- Ussing, N.V. (1912) Geology of the Country around Julianehaab, Greenland. Meddelelser om Grønland **38**, 426 pp.
- VERNON, R.H. (2004) A Practical Guide to Rock Microstructure. Cambridge University Press, Cambridge, United Kingdom, 594 pp.
- Verwey, E.J. (1939) Electronic conduction of magnetite (Fe₃O₄) and its transition point at low temperature. *Nature* **144**, 327–328.
- WAGER, L.R. & BROWN, G.M. (1968) Layered Igneous Rocks. Oliver and Boyd, London, United Kingdom, 588 pp.
- WAGER, L.R. & DEER, W.A. (1939) Geological investigations in East Greenland. Part III. The petrology of the Skaergaard intrusion, Kangerdlussuaq, East Greenland. *Meddelelser om Grønland* 105(4).
- WIEDENMANN, A., REGNARD, J.R., FILLION, G., & HAFNER, S. (1986) Magnetic properties and magnetic ordering of the orthopyroxenes. *Journal of Physics C: Solid State Physics* 19, 3683–3695.
- WINKLER, A., FLORINDO, F., & SAGNOTTI, L. (1996) Inverse to normal fabric transition in an upper Miocene marly sequence from Tuscany, Italy. *Geophysical Research Letters* 23, 909–912.
- Received February 27, 2024. Revised manuscript accepted July 15, 2024.
- This manuscript was handled by Associate Editor Ciro Cucciniello and Editor Stephen Prevec.